

# Molecular Embedding-Based Algorithm Selection in Protein-Ligand Docking

Jiabao Brad Wang<sup>1</sup>, Siyuan Cao<sup>1</sup>, Hongxuan Wu<sup>1</sup>,  
Yiliang Yuan<sup>2</sup>, Mustafa Mısırlı<sup>1\*</sup>

<sup>1\*</sup>Division of Natural and Applied Sciences, Duke Kunshan University,  
8 Duke Av., Suzhou, 215316, Jiangsu, China.

<sup>2</sup>Machine Learning Department, Mohamed bin Zayed University of  
Artificial Intelligence, Building 1B, Masdar City, Abu Dhabi, UAE.

\*Corresponding author(s). E-mail(s):

[mustafa.misir@dukekunshan.edu.cn](mailto:mustafa.misir@dukekunshan.edu.cn);

Contributing authors: [jb.wang@dukekunshan.edu.cn](mailto:jb.wang@dukekunshan.edu.cn);  
[siyuan.cao@dukekunshan.edu.cn](mailto:siyuan.cao@dukekunshan.edu.cn); [hongxuan.wu@dukekunshan.edu.cn](mailto:hongxuan.wu@dukekunshan.edu.cn);  
[yiliang.yuan@mbzuai.ac.ae](mailto:yiliang.yuan@mbzuai.ac.ae);

## Abstract

Selecting an effective docking algorithm is highly context-dependent, and no single method performs reliably across structural, chemical, or protocol regimes. We introduce MolAS, a lightweight algorithm selection system that predicts per-algorithm performance from pretrained protein-ligand embeddings using attentional pooling and a shallow residual decoder. With only hundreds to a few thousand labelled complexes, MolAS achieves up to 15% absolute improvement over the single-best solver (SBS) and closes 17–66% of the Virtual Best Solver (VBS)–SBS gap across five diverse docking benchmarks. Analyses of reliability, embedding geometry, and solver-selection patterns show that MolAS succeeds when the oracle landscape exhibits low entropy and separable solver behaviour, but collapses under protocol-induced hierarchy shifts. These findings indicate that the main barrier to robust docking AS is not representational capacity but instability in solver rankings across pose-generation regimes, positioning MolAS as both a practical in-domain selector and a diagnostic tool for assessing when AS is feasible.

**Scientific contribution.** The results with MolAS indicate that the main barrier to robust docking algorithm selection is not representational capacity but instability in solver rankings across workflows. MolAS therefore serves both as a practical in-domain selector for fixed docking pipelines and as a diagnostic tool

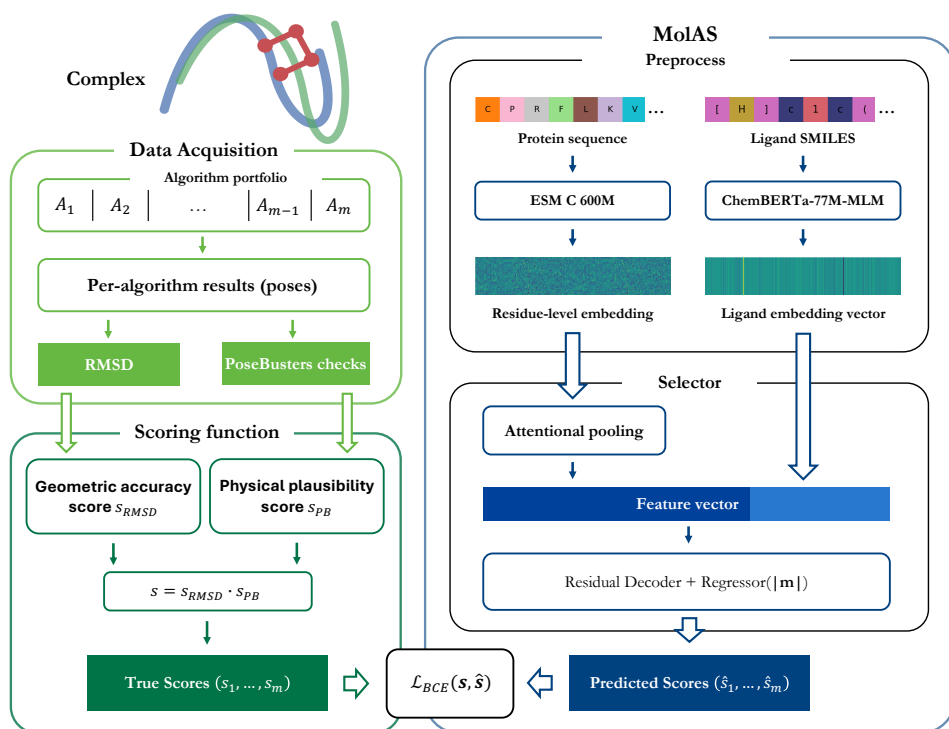


**Fig. 1** Overview of MolAS for workflow-specific molecular docking algorithm selection. (Left) Label data acquisition and scoring. (Right) MolAS model.

for identifying when algorithm selection is intrinsically feasible, merely brittle, or fundamentally ill-posed.

**Graphical abstract.** A visual demo of our work is shown in Fig. 1.

**Keywords:** algorithm selection, cheminformatics, molecular embeddings, pose evaluation, protein-ligand docking, docking benchmarks

## 1 Introduction

Molecular docking is the computational process that predicts the binding configuration of a ligand to its target protein at atomic resolution and is central to structure-based drug discovery [Fan et al., 2019]. Traditional docking pipelines rely on empirical scoring functions coupled with heuristic search [Trott and Olson, 2010, Koes et al., 2013, Hassan et al., 2017], while classical scoring functions have historically spanned physics-based, empirical, and knowledge-based formulations [Ballester and Mitchell, 2010, Cheng et al., 2010, Meng et al., 2011]. These methods balance speed and physical interpretability but often correlate inconsistently with experimental affinities.

Recent machine learning (ML)-based models such as DiffDock [Corso et al., 2022] and SurfDock [Cao et al., 2025a] aim to improve pose generation or scoring by learning protein-ligand interaction patterns directly from data. Despite decades of development, no single method consistently excels across all docking scenarios, reflecting both the *No Free Lunch Theorem* [Wolpert and Macready, 2002] and the profound context dependence of protein-ligand recognition [Yuan and Misir, 2024a].

Algorithm Selection (AS) [Rice, 1976] offers a principled route to adaptivity in such heterogeneous regimes. Rather than committing to a single solver or fixed configuration, AS systems learn to recommend the algorithm predicted to perform best for each instance [Kerschke et al., 2019]. Early AutoML (automated machine learning) systems, such as Auto-WEKA [Thornton et al., 2013] and Auto-sklearn [Feurer et al., 2015], operationalise the AS paradigm at scale through Bayesian optimisation and meta-learning, demonstrating that instance-specific algorithm choice can outperform any fixed method. AS has also proved effective in related molecular modelling tasks like QSAR regression, where meta-learning has shown consistent improvements over single-model baselines across thousands of datasets [Olier et al., 2018].

Chen et al. [2023] introduced the first docking-specific AS framework using the *ALORS* recommender [Misir and Sebag, 2017] to select between AutoDock configurations from tabular features. Subsequent work further explored regression-based parameter tuning [Zayed, 2025]. These works provided valuable demonstrations of feasibility but remained restricted to a single engine, limited descriptors, or narrow protocol settings, yielding moderate gains with limited generality.

A more ambitious line of work extends AS to *cross-algorithm* selection. Our previous study [Yuan and Misir, 2024a] showed that molecular features can support instance-wise recommendations across multiple docking engines, achieving consistent improvements over the single best solver (SBS). Graph-based variants replaced tabular descriptors with protein-ligand graphs to learn structural relationships directly from topology and geometry [Yuan and Misir, 2024b]. Building on these ideas, *GNNAS-Dock* [Yuan and Misir, 2024c] and its multi-criteria extension *MC-GNNAS-Dock* [Cao et al., 2025b] established a unified GNN-driven framework that predicts per-algorithm performance from molecular structure alone, integrating RMSD-based accuracy, PoseBusters plausibility [Buttenschoen et al., 2024], and ranking-aware objectives. Although these systems achieved strong in-domain gains, their evaluations were limited to specific docking pipelines, and their architectural complexity made it difficult to separate true representational gains from effects driven by data distribution, protocol design, or oracle instability. In particular, it remained unclear whether improved AS stems from *better molecular representation* or from *coincidental alignment* between training and evaluation protocols.

The present work introduces **MolAS** (Molecular Embedding-Based Algorithm Selector), a lightweight AS framework designed precisely to interrogate this ambiguity. MolAS replaces graph encoders with pretrained molecular language models for proteins (ESM C [ESM Team, 2024]) and ligands (ChemBERTa [Ahmad et al., 2022]), which already capture substantial structural and chemical information. By pairing these embeddings with a minimal attentional pooler and shallow residual decoder, MolAS isolates the contribution of molecular *representation* from that of *oracle-landscape*

*geometry*, allowing it to test the hypothesis that modern docking AS is primarily constrained by data and protocol variability rather than representational capacity.

We evaluate MolAS on a curated BindingMOAD dataset and across three modern docking benchmarks spanning diverse structural regimes and pose-generation protocols. In most in-domain settings, MolAS consistently outperforms the SBS and closes a significant portion of the virtual best solver (VBS)–SBS gap with only 300–2400 labelled complexes, depending on the benchmark. However, performance deteriorates sharply when training and test protocols differ, demonstrating that MolAS, despite its expressive embeddings, inherits the oracle hierarchy of the workflow on which it is trained. This reveals an important limitation of docking AS that changing the docking protocol effectively changes the AS problem itself.

Ablation studies show that neither deeper encoders nor alternative objective functions provide systematic improvements, reinforcing that solver-hierarchy instability, benchmark-specific oracle entropy, and protocol-induced shifts in ranking dominate performance. Overall, MolAS serves both as a practical selector for workflow-specific docking and as a diagnostic tool that clarifies when docking AS is intrinsically feasible, merely brittle, or fundamentally ill-posed. These findings suggest that robust cross-protocol AS will require explicit modelling of workflow changes rather than further architectural scaling.

## 2 Materials and Methods

### 2.1 Pipeline overview

MolAS is an algorithm selection (AS) system. Let  $\mathcal{X}$  denote a class of problem instances and  $\mathcal{A} = \{A_1, \dots, A_m\}$  a finite set of  $m$  candidate algorithms. An AS system is a mapping

$$S : \mathcal{X} \rightarrow \mathcal{A} \quad (1)$$

that selects, for each  $\mathbf{x} \in \mathcal{X}$ , an algorithm expected to perform well under a task-specific performance measure  $\phi : \mathcal{A} \times \mathcal{X} \rightarrow \mathbb{R}_{\geq 0}$  [Rice, 1976]. In practice,  $\phi$  is unknown and approximated by a learned model  $\hat{\phi} : \mathcal{A} \times \mathcal{X} \rightarrow \mathbb{R}_{\geq 0}$ . The system then defines

$$S(x) := \arg \max_{A \in \mathcal{A}} \hat{\phi}(A, \mathbf{x}), \quad (2)$$

thereby inducing selection via performance prediction. Often, it is modelled  $(\hat{\phi}(A_1, \mathbf{x}), \dots, \hat{\phi}(A_m, \mathbf{x})) = \hat{\phi}(\mathbf{x}) = g(f(\mathbf{x}))$  for a feature extractor (encoder)  $f : \mathcal{X} \rightarrow \mathbb{R}^d$  and performance predictor (decoder)  $g : \mathbb{R}^d \rightarrow \mathbb{R}^m$  learned to reconstruct the performance/score labels  $\mathbf{s} \in \mathcal{S}$ , yielding the composition

$$S = \arg \max \circ g \circ f. \quad (3)$$

Such a system, as shown in Fig. 2, induces a total ranking over  $\mathcal{A}$  for each problem instance by its characteristics, with selection yielding the top-ranked algorithm. In our work, each  $\mathbf{x} = (\mathbf{x}_P, \mathbf{x}_L)$  represents the input pair constructed from a protein-ligand pair (§2.2.3),  $f, g$  are learned by an attentional pooler and a residual MLP

decoder respectively (§2.3), and the target performance metrics are formulated with a physics-inspired composite scoring function (§2.4).

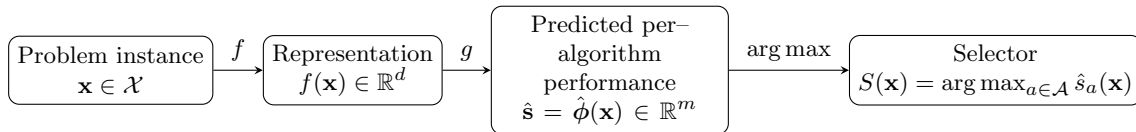


**Fig. 2** Schematic of the algorithm selection mapping in the sense of Rice [1976]. Each instance  $\mathbf{x}$  is mapped to a feature vector  $f(\mathbf{x})$ , from which a predictor  $g$  produces a vector  $\hat{\mathbf{s}}$  of estimated performances for all algorithms in the portfolio  $\mathcal{A}$ . The selector chooses the algorithm with maximal predicted performance.

**Fig. 3** Candidate docking algorithms for algorithm selection

Method	Type	Central mechanism
Smina [Koes et al., 2013]	Classical	Vina with empirical scoring and local search
Qvina-W [Hassan et al., 2017]	Classical	Vina with fast stochastic global optimisation
DiffDock [Corso et al., 2022]	ML-based	Diffusion model for direct pose generation
DiffDockL [Corso et al., 2024]	ML-based	DiffDock with flexible ligand modeling
SurfDock [Cao et al., 2025a]	ML-based	$SE(3)$ -equivariant diffusion GNN
Gnina [McNutt et al., 2021]	ML-based	3D CNN-based rescoring of docking poses
Uni-Mol Docking V2 [Alcaide et al., 2025]	ML-based	Transformer on atomic coordinates with pretraining
KarmaDock [Zhang et al., 2023]	ML-based	$SE(3)$ -equivariant attention

## 2.2 Datasets and preprocessing

### 2.2.1 Dataset

A proper AS dataset involves problem instances, protein-ligand pairs here,  $\mathcal{X} = \{\mathbf{x}_1, \dots, \mathbf{x}_n\}$  and score targets  $\mathcal{S} \in \mathbb{R}^{n \times m}$  that contain per-instance, per-algorithm performance data. Acquiring such data is inherently challenging due to the limitations of available data that differs from the training data of the candidate algorithms and the substantial costs required to evaluate each docking algorithm across all instances in the dataset. This necessitates a strategic selection of both representative molecular instances and algorithms. This study therefore employs a curated portfolio of eight methodologically diverse docking algorithms, selected to represent either state-of-the-art techniques and established baselines, as summarised in Table 3.

Since most of these algorithms have parsed *PDBBind* [Liu et al., 2017] as the training set, we evaluate them on *BindingMOAD* [Hu et al., 2005], a comprehensive dataset of experimentally determined protein-ligand complexes. A subset of the performance results over around 3000 cases (thereafter, *MOAD-curated*) is then curated so that each algorithm demonstrates strong performance in certain docking scenarios, to ensure the presence of a non-trivial selection problem.

### 2.2.2 Extra benchmarks

In addition to MOAD-curated, two external benchmarks, *PoseX* [Jiang et al., 2025] and *PoseBusters* [Buttenschoen et al., 2024] are included to assess the model’s performance over distinct data distributions.

*PoseX* is a docking benchmark including **718 self-docking** cases (*PoseX-SD*) and **1312 cross-docking** cases (*PoseX-CD*). Self-docking refers to dock a ligand back into the same protein conformation from which it was crystallised. Cross-docking docks ligands into non-cognate protein conformations, introducing backbone and side-chain differences that more closely resemble real-world scenarios where the exact receptor structure is unavailable. These cases, alongside with another benchmark dataset of **85** complexes, *Astex Diverse Set* [Hartshorn et al., 2007], are evaluated across **24** algorithms. These methods span physics-based docking like AutoDock Vina, machine learning-based docking models such as DiffDock and SurfDock, and AI co-folding frameworks that can implicitly orient ligands by joint protein–ligand structure prediction, notably AlphaFold 3. *PoseX* introduces a post-processing step called **relaxation** to be applied to predicted poses. It imposes a lightweight geometry refinement that adjusts atom positions locally to correct clashes and strained conformations while keeping the global docking pose largely unchanged [Jiang et al., 2025]. This step standardises ligand geometry across algorithms without performing full force-field optimisation, making it suitable for algorithm-agnostic comparisons. This design yields a benchmark that captures both near-native and cross-conformation docking scenarios while maintaining comparability across algorithm families.

The *PoseBusters* (V2) benchmark provides a comprehensive validation framework for ligand poses. Its focus extends beyond RMSD accuracy, prioritizing the physical plausibility of docking outputs. It contains **428** complexes and provides predictions from **7** modern docking models. Alongside with the standard output poses, a unified **molecular-mechanics energy minimisation** post-processing step is applied to generate a mirror group of refined poses. During this process, the ligand is optimised with OpenMM using the AMBER ff14SB (protein) and SMIRNOFF/Sage (ligand) force fields while the receptor is held fixed, producing an MM-minimised (MM-min) pose for standardised comparison [Buttenschoen et al., 2024].

We note that several widely used datasets in molecular modelling, such as CASF [Su et al., 2018] and CrossDocked 2020 [Francoeur et al., 2020], are unsuitable for algorithm selection. These benchmarks provide either single-model submissions, aggregated scoring-function results, or affinity labels, but do not release per-algorithm pose predictions across a solver portfolio. Since AS requires instance-level performance profiles for multiple algorithms to define SBS, VBS, and supervised training labels, such datasets cannot be used without recomputing all predictions under a controlled protocol. For this reason, our evaluation focuses on *PoseX* and *PoseBusters*.

### 2.2.3 Preprocessing

Protein inputs are represented at the residue level. For each protein, we encode per-residue embeddings using **ESM C 600M** [ESM Team, 2024], yielding a sequence of

vectors  $\mathbf{x}_P \in \mathbb{R}^{|\text{residues}| \times 1152}$ . Ligand inputs are encoded using **ChemBERTa-77M-MLM** [Ahmad et al., 2022] to a single pooled embedding  $\mathbf{x}_L \in \mathbb{R}^{384}$ . Both models supply pretrained molecular language representations. ESM C provides residue-level vectors that capture evolutionary and structural regularities, offering a high signal-to-noise representation without requiring supervised pocket annotations. ChemBERTa supplies a chemically informed ligand embedding that captures functional groups and local reactivity patterns more reliably than handcrafted descriptors. Using these pretrained models allows MolAS to operate in the small-data regime by leveraging representations already optimised on large biomolecular corpora, reducing the need for task-specific feature engineering. For each complex, the final input therefore consists of a pair of a protein residue embedding  $\mathbf{x}_P$  and a ligand embedding  $\mathbf{x}_L$ .

---

#### Algorithm 1 MolAS

---

**Require:** Raw data of protein-ligand pairs  $\{(P_i, L_i)\}_{i=1}^n$ ; per-algorithm targets  $\{\mathbf{s}_i \in \mathbb{R}^m\}_{i=1}^n$ ; docking portfolio  $\mathcal{A} = \{a_1, \dots, a_m\}$ ; fusion encoder  $f_\theta$  and decoder head  $g_\theta$  with parameters  $\theta$ .

##### Preprocessing

```

1: for each  $(P_i, L_i)$  do
2:    $\mathbf{x}_{P_i} \leftarrow \text{ESM}(P_i)$ 
3:    $\mathbf{x}_{L_i} \leftarrow \text{ChemBERTa}(L_i)$ 
4: end for
5:  $\mathcal{D} \leftarrow \{((\mathbf{x}_{P_i}, \mathbf{x}_{L_i}), \mathbf{s}_i)\}_{i=1}^n$ 

```

##### Training

```

6: Initialize  $\theta$ .
7: for mini-batch  $\mathcal{B} \subset \mathcal{D}$  do
8:   for  $((\mathbf{x}_P, \mathbf{x}_L), \mathbf{s}) \in \mathcal{B}$  do
9:      $\mathbf{z} \leftarrow f_\theta(\mathbf{x}_P, \mathbf{x}_L)$ 
10:     $\hat{\mathbf{s}} \leftarrow g_\theta(\mathbf{z}) \in \mathbb{R}^m$ 
11:   end for
12:   Compute loss  $\mathcal{L}_{\text{BCE}}(\theta; \mathcal{B})$  between  $\{\hat{\mathbf{s}}\}$  and  $\{\mathbf{s}\}$ .
13:    $\theta \leftarrow \theta - \eta \nabla_\theta \mathcal{L}_{\text{BCE}}$ 
14: end for

```

##### Inference (selection)

```

15: function  $S(\mathbf{x}_P, \mathbf{x}_L)$ 
16:    $\hat{\mathbf{s}} \leftarrow g_\theta(f_\theta(\mathbf{x}_P, \mathbf{x}_L)) \in \mathbb{R}^m$ 
17:    $j^* \leftarrow \arg \max_{j \in \{1, \dots, m\}} \hat{s}_j$ 
18:   return  $a_{j^*}$ 
19: end function

```

---

## 2.3 Model architecture

The **encoder**  $f$  consists of an attentional pooler applied to the protein embeddings, followed by a ligand–protein fusion module. The attention layer compresses the residue-level representations into a single protein vector, which is then concatenated with the ligand embedding and linearly projected into a lower-dimensional joint space.

Inspired by the demonstrated stability and variation preservation of ResNet [He et al., 2020], the fused representation is passed to a residual multilayer perceptron (MLP) that outputs per-algorithm performance scores. The **decoder**  $g$  comprises three consecutive residual blocks, each containing a linear layer, batch normalisation, and ReLU activation with a skip connection. The outputs of all residual blocks are concatenated and processed by a final linear projection head to produce the predicted score vector  $\hat{\mathbf{s}} \in \mathbb{R}^m$  over the algorithm portfolio.

The binary cross-entropy (BCE) loss is used for calibration of the true scores  $\mathbf{s}$  with logits  $\hat{\mathbf{s}}$ , defined by

$$\mathcal{L}_{\text{BCE}}(\hat{\mathbf{s}}, \mathbf{s}) = - \sum_{a \in \mathcal{A}} \left[ s_a \log \sigma(\hat{s}_a) + (1 - s_a) \log(1 - \sigma(\hat{s}_a)) \right],$$

where  $\sigma$  is the logistic sigmoid. Training minimises the mean BCE over mini-batches.

The procedures of MolAS are summarised in Alg. 1.

## 2.4 Scoring function

### 2.4.1 Geometric accuracy

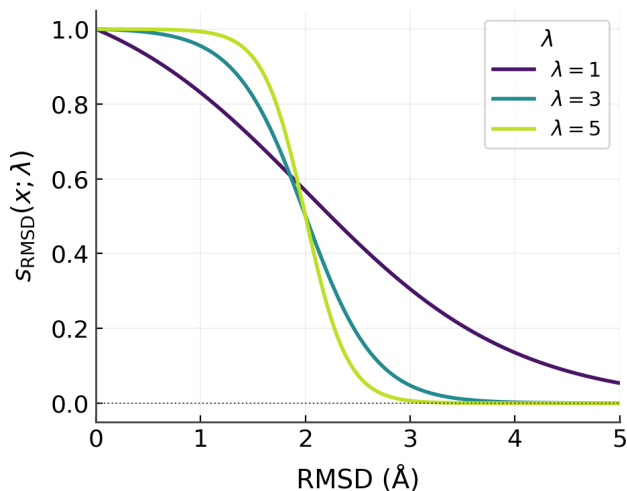


**Fig. 4**  $s_{\text{RMSD}}(x; \lambda)$  curves when  $\lambda \in \{1, 3, 5\}$ .



RMSD measures the spatial distance from a predicted pose to the crystal reference in Angstrom ( $\text{\AA}$ ). A pose with  $\text{RMSD} \leq 2 \text{\AA}$  is typically considered geometrically valid. The exponential scoring function used by MC-GNNAS-Dock [Cao et al., 2025b] captures this diminishing returns in RMSD improvements but assigns zero value to all poses with RMSD above a hard threshold ( $M = \ln 11 \approx 2.39$ ), thereby neglecting informative differences between moderately poor poses. To address this, we propose a smooth sigmoid-based score function:

$$s_{\text{RMSD}}(x; \lambda) = \frac{1 + e^{-2\lambda}}{1 + e^{\lambda(x-2)}}, \quad \lambda > 0, \quad (4)$$

which is centred at the critical threshold of  $2 \text{\AA}$ , where the maximum gradient occurs, ensuring the model rewards borderline improvements most strongly, while gains or losses away from this boundary yield diminishing marginal effect (Fig. 4). The parameter  $\lambda$  controls the sensitivity of the score to changes in RMSD, and is set to  $\lambda = 3$  with an ablation conducted in §3.3.

#### 2.4.2 Physicochemical plausibility.

The PB-validity score (PoseBusters-validity) of a pose is evaluated by a binary accept-reject gate that mirrors current practice in crystallographic validation:

$$s_{\text{PB}} = \begin{cases} 1 & \text{passes all 18 PoseBusters checks,} \\ 0 & \text{otherwise,} \end{cases} \quad (5)$$

which ensures that no geometrically plausible yet chemically impossible pose can receive a decent score. Our final score is then the RMSD score gated by PB-validity

$$s = s_{\text{RMSD}} \cdot s_{\text{PB}}. \quad (6)$$

## 2.5 Experimental Setup

### 2.5.1 Implementation details

All models are implemented in Python using PyTorch. The code and weights of ESM C 600M model are acquired from Lin et al. [2025]. Models are trained with the Adam optimiser using a cosine learning-rate schedule and early stopping based on validation accuracy. All experiments are conducted on a dual-socket server with two AMD EPYC 7763 CPUs and 8 NVIDIA RTX 3090 GPUs, running Ubuntu 22.04.5 LTS.

### 2.5.2 Reporting protocol

We evaluate MolAS under two standard AS baselines. The **Single Best Solver (SBS)** is the single docking method achieving the highest mean performance on the tested benchmark. The **Virtual Best Solver (VBS)** is an oracle that chooses the highest-scoring method for each complex, i.e., the theoretical maximum or limit. In addition to absolute accuracy, we report the fraction of the **VBS-SBS gap closed**, denoted as

$\% \frac{AS-SBS}{VBS-SBS}$ , which quantifies the actionable improvement achieved by MolAS relative to the upper bound imposed by the portfolio.

For interpretability, some results involve **Selected@K** and **VBS@K**, which summarise the behaviour of the selector beyond the top choice. Here, Selected@K denotes the *algorithm* ranked  $K^{th}$  by MolAS selection frequency over the tested benchmark, e.g., the second most frequently selected algorithm when  $K = 2$ . VBS@K denotes a virtual *selector* that selects the  $K^{th}$  best algorithm for each instance.

Two evaluation regimes are used. For in-domain learning, each benchmark is evaluated using a 5-fold split with an 8–2 train–test ratio per fold; results report the mean over all folds. For cross-benchmark learning, the entire source benchmark is used for training and the entire target benchmark for testing, with no overlap between complexes. All metrics are reported for success rates of both strict ( $RMSD \leq 1 \text{ \AA}$  & PB-valid) and relaxed ( $RMSD \leq 2 \text{ \AA}$  & PB-valid) success criteria.

## 3 Results

We report MolAS’ in-domain performance (§3.1.1), analyse its failure cases and their underlying causes (§3.1.2), and evaluate cross-benchmark generalisation (§3.1.3). We further compare MolAS with the prior GNN-based MC-GNNAS-Dock framework (§3.2) and provide architectural and data-driven ablations (§3.3).

### 3.1 Benchmark Performance

#### 3.1.1 In-domain learning

Table 1 reports within-distribution performance across benchmarks. On the composite *MOAD-curated* set, MolAS attains success rates of **50.01%** under the strict ( $RMSD \leq 1 \text{ \AA}$  & PB-valid) criterion and **74.68%** under the relaxed ( $RMSD \leq 2 \text{ \AA}$  & PB-valid) criterion, improving over the SBS (Uni-Mol Docking V2) by **6.6%** and **6.51%** respectively. These gains close roughly **17–23%** of the VBS–SBS gap. Improvements are more pronounced on *PoseX-CD*, where MolAS closes approximately **45%** and **61%** of the gap under the strict and relaxed criteria. On the hybrid *PoseX + Astex* dataset, absolute gains of **8.38%** (strict) and **5.72%** (relaxed) correspond to **21–24%** gap closure, indicating robust behaviour under substantial structural and chemical diversity when trained on comparably heterogeneous data. All these improvements above SBS are statistically significant at  $p < 0.05$  (paired test).

The improvements on *PoseBusters* from (**34.3%**, **51.2%**) to (**36.7%**, **54.9%**) are relatively marginal. A similar pattern is also seen on *PoseX-SD*, where MolAS performs remarkably closely SBS – (**50.1%**, **74.2%**) v.s. (**51.6%**, **74.6%**). This dataset contains a high proportion of near-rigid receptor complexes with limited chemical and structural diversity, resulting in weaker correlation between protein embeddings and algorithm performance. The reduced gain here suggests that the advantage of learned molecular embeddings becomes less pronounced when docking difficulty is dominated by local energy optimisation rather than global geometric variation. Nevertheless, performance

**Table 1** Averaged 5-fold MolAS performance v.s. SBS across benchmarks. Columns list PoseBusters-validated pose rates within 1 Å and 2 Å RMSD, and the VBS-SBS gap closed. Bold marks improvement over SBS, and an improvement with \* indicates  $p < 0.05$  (paired test between MolAS and SBS).

Dataset	Post-process	SBS	(% )RMSD $\leq 1$ Å & PB-valid			(% )RMSD $\leq 2$ Å & PB-valid		
			SBS	MolAS	$\% \frac{AS-SBS}{VBS-SBS}$	SBS	MolAS	$\% \frac{AS-SBS}{VBS-SBS}$
With-and-without relaxation trained together								
MOAD-curated	Mixed	Uni-Mol	43.41	<b>50.01*</b>	<b>17.42</b>	68.17	<b>74.68*</b>	<b>22.40</b>
PoseX + Astex	Mixed	SurfDock (relax)	50.24	<b>58.61*</b>	<b>21.42</b>	74.08	<b>79.8*</b>	<b>24.24</b>
PoseX-SD	Mixed	SurfDock (relax)	50.08	<b>51.62</b>	<b>3.66</b>	74.21	<b>74.63</b>	<b>1.67</b>
PoseX-CD	Mixed	SurfDock (relax)	49.08	<b>66.39*</b>	<b>45.50</b>	73.02	<b>87.50*</b>	<b>61.28</b>
PoseBusters	Mixed	AutoDock	34.34	<b>36.69</b>	<b>8.90</b>	51.17	<b>54.91</b>	<b>11.87</b>
With-and-without relaxation trained separately								
PoseX + Astex	No	Boltz1x	42.48	<b>57.05*</b>	<b>32.12</b>	61.02	<b>76.58*</b>	<b>42.67</b>
	Relaxation	SurfDock (relax)	50.24	<b>58.94*</b>	<b>23.32</b>	74.08	<b>80.84*</b>	<b>28.99</b>
PoseX-SD	No	Uni-Mol	40.73	<b>43.51</b>	<b>5.56</b>	60.53	<b>62.62</b>	<b>5.41</b>
	Relaxation	SurfDock (relax)	50.08	<b>50.22</b>	<b>0.37</b>	74.21	73.93	-1.10
PoseX-CD	No	Boltz1x	44.82	<b>61.66*</b>	<b>41.48</b>	65.16	<b>83.38*</b>	<b>58.29</b>
	Relaxation	SurfDock (relax)	49.08	<b>66.99*</b>	<b>49.27</b>	73.02	<b>88.41*</b>	<b>66.43</b>
PoseBusters	No	AutoDock	34.34	<b>36.44</b>	<b>11.67</b>	51.17	<b>53.97</b>	<b>9.83</b>
	MM-min	Gold (MM-min)	27.58	26.87	-3.24	45.10	<b>45.81</b>	<b>2.34</b>

remains close to parity, and the model retains its lead on the corresponding cross-docking subset (*PoseX-CD*), indicating that MolAS is more sensitive to chemical heterogeneity than to docking rigidity.

To further quantify the effect of structural relaxation, we compared models trained on mixed versus post-process-separated datasets using the VBS-SBS gap closed as the metric of interest, as SBS performance varies between regimes. The post-process flag indicates similar trends. For the hybrid *PoseX + Astex* benchmark, separating the relaxation regimes yielded higher performance in both subsets, suggesting that independent modelling of (relax) and un(relax) structures slightly improves consistency. For *PoseX-SD*, some non-uniform trends have been seen: the non-(relax) regime led to an incremental improvement in both success rates respectively, exceeding the mixed-data baseline, while the (relax) regime was marginally worse than the mixed setting. However, given the small magnitude, these are rather considered insignificant fluctuations. *PoseX-CD* maintained its strong performance across all conditions, also with only minor fluctuations that were not systematic across folds. In contrast, on *PoseBusters*, MolAS performed comparably to mixed data in the non-(MM-min) subset but showed a marked drop under the (MM-min) regime, likely reflecting the different energy-minimization procedure used in that dataset.

Overall, MolAS demonstrates strong performances which outperform the SBS over most tested scenarios remains robust across relaxation regimes, underscoring the AS

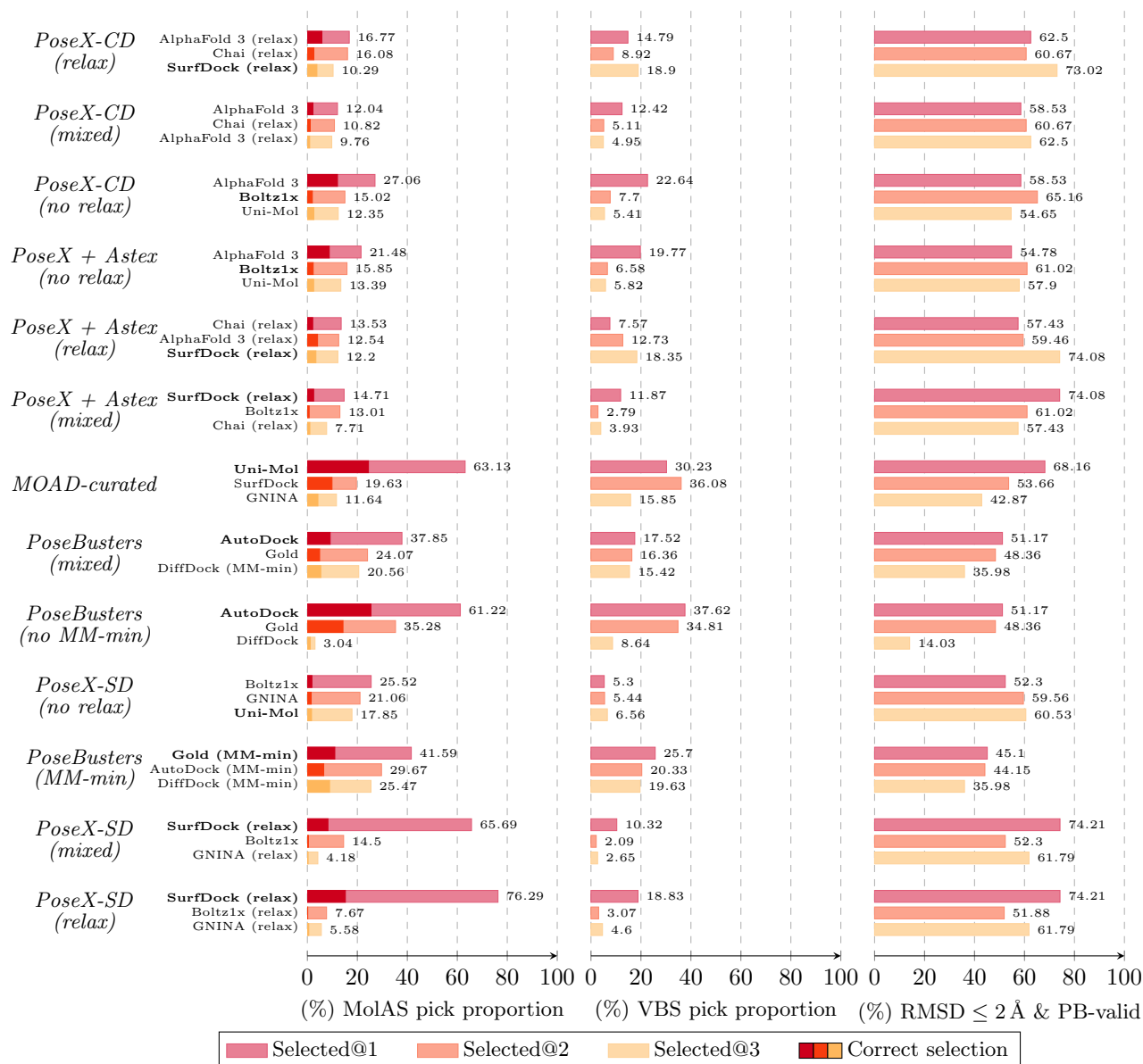


**Fig. 5** The selection frequencies by MolAS (left bar chart) and by the VBS (middle bar chart) and their success rates under the relaxed ( $\text{RMSD} \leq x \text{ \AA}$  & PB-valid) criterion (right bar chart) of the **top-3 selected algorithms by MolAS** in the concatenated 5-fold results over benchmarks. The benchmarks are ordered descending based on the VBS-SBS gap closed by MolAS under the relaxed criterion. The correct picks by MolAS (those that accords with the VBS) are coloured in deeper colours and the SBS method for each benchmark is in **bold**.

system’s consistent ability to bridge solver redundancy and achieve reproducible in-domain improvements across chemically diverse docking conditions. That said, it

**Table 2** Summary of embedding-space statistics and oracle-landscape properties across benchmarks. Cluster tightness and Silhouette score quantify per-algorithm embedding dispersion and separability. VBS score and VBS entropy summarise the oracle success rate and the distribution of oracle-best algorithms.

Dataset	Cluster tightness	Silhouette score	VBS score	VBS entropy
MOAD-curated	3.305	-0.036	0.867	2.395
PoseX + Astex	2.709	-0.143	0.956	4.699
PoseX-SD	2.960	-0.173	0.972	4.675
PoseX-CD	2.431	-0.183	0.944	4.590
PoseBusters	2.982	-0.047	0.763	3.205

shows a clear data-specific failure pattern (e.g., on *PoseX-SD*), which is investigated subsequently.

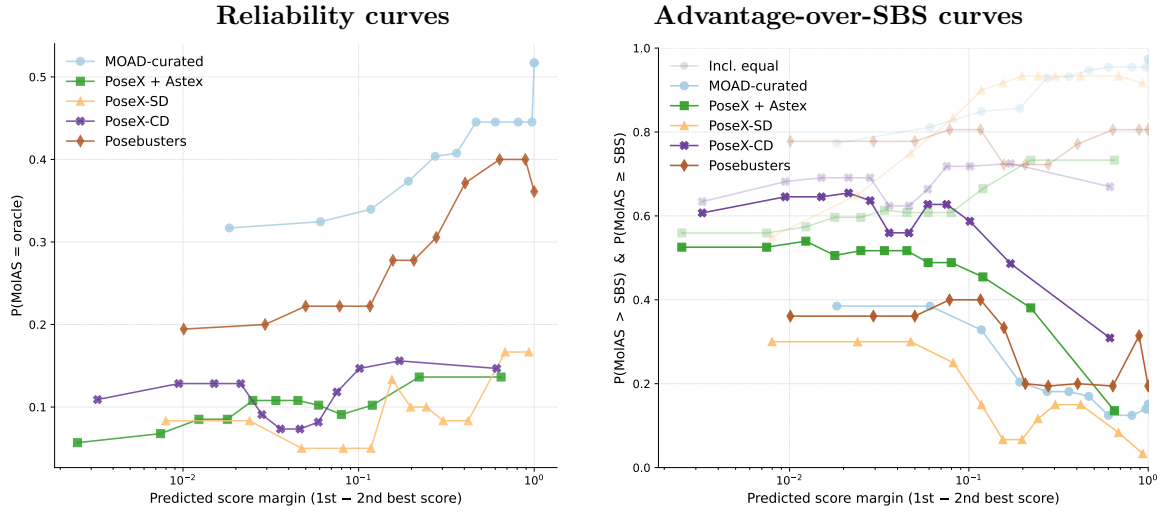


**Fig. 6** (Left) reliability curves showing the probability that MolAS matches the oracle as a function of predicted score margin (12 equal-mass bins). (Right) Advantageness curves obtained by replacing reliability (MolAS accords with VBS) with advantageness over SBS. Solid lines correspond to MolAS outperforming SBS ( $s_{\text{MolAS}} > s_{\text{SBS}}$ ) and faded lines for MolAS performing as well as SBS ( $s_{\text{MolAS}} \geq s_{\text{SBS}}$ ). Thereby, the y-axis indicates the probability that MolAS achieves higher true score than the SBS within each margin bin.

### 3.1.2 Operational boundaries of MolAS

The behaviour of MolAS deteriorates on PoseX-SD and PoseBusters once relaxation is enabled and in several cross-benchmark settings. We therefore examined these regimes in more detail, (i) focusing on how the selector distributes its choices across the portfolio, (ii) whether those choices are conditionally reliable, and (iii) how the embedding space and algorithm landscape affect the performance.

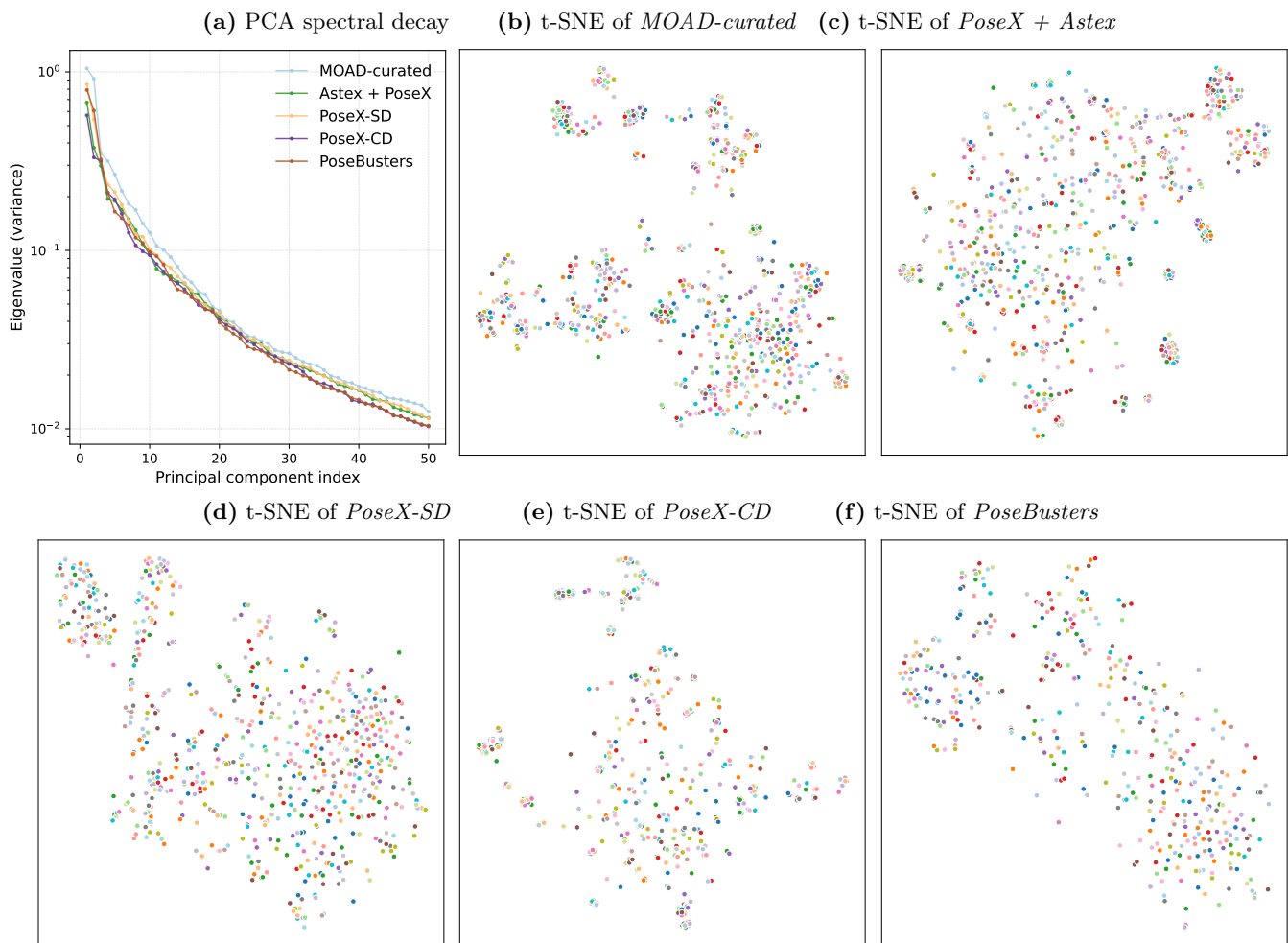


**Fig. 7** (a) Eigenvalue spectra via PCA. (b - f) t-SNE visualisations of embedding spaces across benchmarks. Each panel shows a 2D projection of embedding clusters coloured by their oracle-selected algorithm.

Fig. 5 displays the selection frequencies and performances of the top-selected algorithms across benchmarks ordered by MolAS' performance. Taken together, these benchmarks form a clear spectrum of selection patterns. At one end lies a collapse of MolAS' selection distribution onto a single dominant solver, typically the solver most frequently chosen by the VBS, whereas the VBS itself generally exhibits a much flatter, multi-modal preference structure. This behaviour characterises benchmarks on which MolAS fails to improve upon the SBS. For example, in *PoseX-SD (relax)*, MolAS selects **SurfDock (relax)** in roughly **75%** of test cases, whereas the VBS uses it in fewer than **20%** of instances, with the second most frequent MolAS choice trailing by over 60 percentage points. Similar collapses occur in *PoseX-SD (mixed)* and *PoseBusters (MM-min)*.

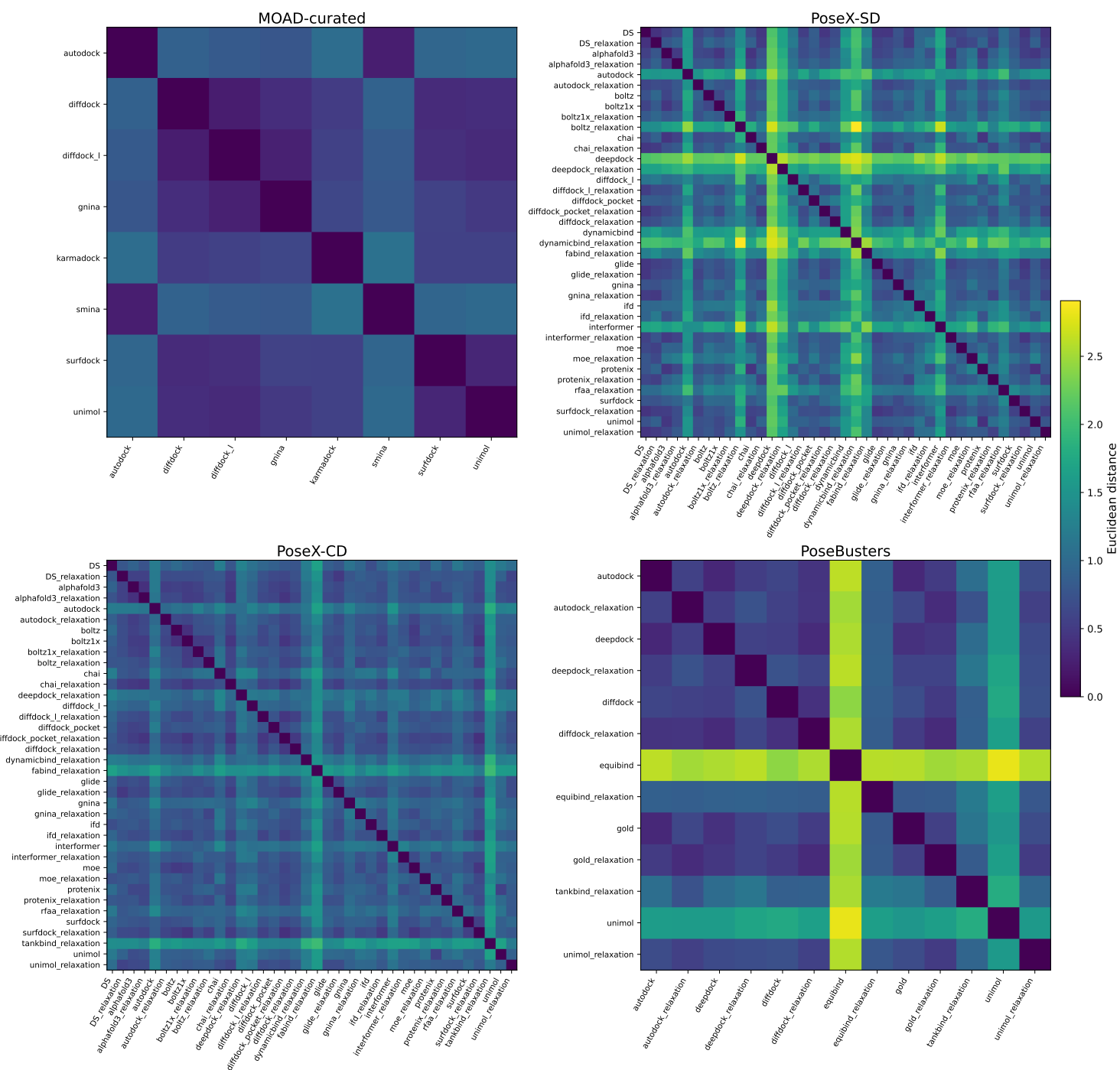


**Fig. 8** Pairwise Euclidean distances between embedding-space centroids of docking algorithms for each benchmark. Darker values indicate smaller distances; diagonal entries are zero by definition. Separate panels show MOAD-curated, PoseX-SD, PoseX-CD, and PoseBusters.

At the opposite end of the spectrum - benchmarks where MolAS substantially outperforms the SBS - the selection distribution is more balanced. The most frequently selected method is either not the dominant VBS choice (as in *MOAD-curated* and *PoseX-CD (relax)*), or its frequency closely mirrors the VBS’ own distribution (as in *PoseX-CD (no relax)*). Between these two extremes lie the mid-performing benchmarks, which either overweight suboptimal solvers more than the oracle would (*PoseX-SD (no relax)*) or exhibit a large top-3 block dominated by the VBS’ Selected@1 (*PoseBusters (mixed/no MM-min)*).

Across all benchmarks, MolAS achieves per-selection precision *below 50%*, yet still produces substantial gains on several datasets. This apparent discrepancy arises because precision is not decisive when the **oracle landscape is relatively flat**: if several algorithms achieve similar oracle scores, selecting any of the top two or three solvers often yields accuracy well above the SBS. In such ‘healthy’ portfolios, MolAS can outperform the SBS even when it misidentifies the oracle-best algorithm, provided its choices remain in the top region of the solver hierarchy. Consistently, VBS@2 and VBS@3 already exceed SBS performance on these benchmarks, indicating that the oracle advantage is distributed across multiple solvers rather than concentrated in a single method (Appendix A.1).

We then examined **reliability** and **advantageness** over SBS each as a function of the score margin between the top-ranked and second-ranked algorithms by MolAS (Fig 6). Across benchmarks, these curves reveal a consistent interaction between MolAS’ score margin, its tendency to default to the SBS, and its ability to exceed it. In low-margin regions, MolAS seldom matches the oracle but often outperforms the SBS, particularly on *PoseX-CD* and *PoseX + Astex*, indicating that when no solver is strongly favoured, the selector explores alternatives that are, on average, better than the SBS. As the margin increases, the pattern reverses: reliability rises (most clearly on *MOAD-curated* and *PoseBusters*), while the probability of outperforming the SBS declines, showing that large margins primarily reflect confident *re-selection* of the SBS. *PoseBusters* remains unusual in displaying stable ‘as-good-as-SBS’ performance across margins. Combined with the frequency collapses in Fig. 5, these results indicate that margin is a benchmark-dependent, partially calibrated confidence signal: high margins are trustworthy only when oracle diversity is low or the portfolio is small, and are least informative on the chemically richer PoseX benchmarks.

The investigation then turns to the embedding space of the benchmarks, specifically with the **PCA** (principal component analysis) **spectra** and **t-SNE** (t-distributed stochastic neighbour) projections of the pooled protein + ligand embeddings (Fig. 7). The PCA spectra are almost identical across benchmarks, with similar eigenvalue decay and no sign of low-rank collapse, indicating embeddings being of comparable intrinsic dimensionality, which exempts a gross loss of capacity from causing failures on *PoseX-SD* and *PoseBusters*. t-SNE projections and the cluster statistics in Table 2 further refine this picture. All benchmarks show multi-lobed clouds rather than clean algorithm clusters, as expected since embeddings are not trained to separate solvers. Still, *MOAD-curated* and *PoseBusters* contain several relatively compact ‘islands’, where *PoseX* benchmarks appear more entangled with fewer dominant regions. This is consistent with their silhouette coefficient (−0.173 and −0.183 in Table 2), indicating



poor oracle-cluster separability. These results suggest that MolAS’ difficult regimes stem from subtle geometric and distributional effects in the embedding space, not from a simple collapse of its feature spectrum.

The inter-algorithm centroid-distance heat-maps (Fig. 8) provide a complementary view at the solver level. On *MOAD-curated*, distances between centroids are moderate and relatively homogeneous, reflecting a compact, low-entropy portfolio in which only a handful of methods are frequently optimal. For *PoseX*, the distance matrices become denser and show repeated block patterns, consistent with many algorithms occupying overlapping regions of the embedding space and sharing similar oracle performance. *PoseBusters* is structurally different: **EquiBind**, and to a less extent **Uni-Mol**, each forms a distinct high-distance block, while the remaining solvers cluster more tightly.

Table 2 summarises *algorithm separability* in the embedding space, quantified by **cluster tightness** (mean within-algorithm embedding distance) and **silhouette score** (relative intra- vs inter-cluster separation), and *the structure of the oracle landscape* captured by the oracle success rate (**VBS score**) and the diversity of oracle winners (**VBS entropy**). *PoseX-SD* is the limiting case for high oracle score and entropy yet the poorest embedding separability, where MolAS collapses to a near single-solver strategy. *MOAD-curated* sits at the opposite end for lower entropy, better separability, and correspondingly high gap-closure and good reliability. *PoseBusters* combines a low oracle ceiling with moderate entropy and separability, explaining why selection yields only incremental gains and reacts strongly to changes in energy minimisation.

In summary, MolAS is most effective when multiple algorithms are competitive and occupy at least partially distinct embedding regions. When embeddings fail to separate algorithms, the selector becomes overconfident and defaults to a near-SBS policy. This defines a clear operational boundary for learned docking algorithm selection.

### 3.1.3 Cross-benchmark generalisation

The cross-benchmark results in Table 3 indicate that MolAS does not achieve meaningful generalisation across docking distributions. Although a few *PoseX SD*→*CD* transfers produce small positive gap closures (3.79% and 4.19% in the mixed regime, 2.50% in the relax-only regime), none of these improvements reach statistical significance, and all are numerically marginal. Without statistical support, these fluctuations are better interpreted as noise rather than evidence of generalisable behaviour.

In contrast, the majority of cross-distribution transfers show consistent and large degradations, including around 13% to 48% *VBS-SBS gap widening* for *PoseX CD*→*SD*, 7% to 84% for *PoseX-SD*→*Astex*, and up to 108% gap widening for *PoseX-CD*→*Astex*. These failures span both the 1 Å and 2 Å thresholds and persist regardless of whether relaxation and non-relaxation data are trained jointly or separately. The pattern is systematic that whenever the target benchmark differs materially in docking protocol, pose-generation behaviour, or algorithm hierarchy, MolAS collapses towards the SBS baseline or worse. This behaviour aligns with the diagnostics presented in our failure analysis. Across poorly transferring regimes, the selector’s

**Table 3** Cross-benchmark results of MolAS performance v.s. SBS (of the test set) across benchmark pairs. Columns list PoseBusters-validated pose rates within 1 Å and 2 Å RMSD, and the VBS-SBS gap closed. Bold marks improvement over SBS, and an improvement with \* indicates  $p < 0.05$  (paired test between MolAS and SBS).

Train	Test	Post-Process	SBS	% $\leq 1 \text{ \AA}$ & PB-valid			% $\leq 2 \text{ \AA}$ & PB-valid		
				SBS	MolAS	% $\frac{AS-SBS}{VBS-SBS}$	SBS	MolAS	% $\frac{AS-SBS}{VBS-SBS}$
With-and-without relaxation trained together									
PoseX-SD	PoseX-CD	Mixed	SurfDock (relax)	49.09	<b>50.53</b>	<b>3.79</b>	73.02	<b>74.01</b>	<b>4.19</b>
PoseX-CD	PoseX-SD	Mixed	SurfDock (relax)	50.07	44.63	-12.96	74.2	62.2	-47.81
PoseX-SD	Astex	Mixed	SurfDock (relax)	69.41	65.88	-11.54	89.41	87.06	-22.19
PoseX-CD	Astex	Mixed	SurfDock (relax)	69.41	65.88	-11.54	89.41	82.53	-66.67
With-and-without relaxation trained separately									
PoseX-SD	PoseX-CD	No Relaxation	Boltz1x	44.82	40.7	-10.14	65.17	59.98	-16.61
			SurfDock (relax)	49.09	<b>50.0</b>	<b>2.50</b>	73.02	72.94	-0.35
PoseX-CD	PoseX-SD	No Relaxation	Uni-Mol	40.73	38.91	-3.64	60.53	57.04	-9.03
			SurfDock (relax)	50.07	42.68	-18.53	74.2	59.55	-58.37
PoseX-SD	Astex	No Relaxation	Uni-Mol	77.65	58.82	-84.25	85.88	75.29	-75.00
			SurfDock (relax)	69.41	67.06	-7.68	69.41	87.06	-22.19
PoseX-CD	Astex	No Relaxation	Uni-Mol	77.65	56.47	-94.77	85.88	70.59	-108.29
			SurfDock (relax)	69.41	67.06	-7.68	69.41	81.18	-77.71

output distribution contracts sharply onto a single dominant method (e.g. SurfDock (relax) for many cases), diverging from the oracle distributions of the target benchmarks.

Taken together, these observations show that MolAS does not learn an invariant mapping from molecular geometry to optimal docking algorithm. Instead, it fits workflow-specific priors tied to the training protocol’s pose-generation mechanisms and scoring landscape. Once these priors no longer hold (e.g., cross-benchmark scenarios), the learned decision surface becomes misaligned with the true oracle hierarchy, leading to systematic negative transfer.

The cross-benchmark asymmetry is therefore not incidental but reflects a limitation that algorithm selection in docking learns algorithm performance distribution thus is inherently protocol-dependent, and MolAS inherits this dependency.

### 3.2 Comparison to MC-GNNAS-Dock

We benchmarked MC-GNNAS-Dock [Cao et al., 2025b] across the same distributions to assess whether MolAS offers a substantive improvement over a heavier, GNN-based selector. As summarised in Fig. 9, MolAS consistently outperforms MC-GNNAS-Dock across all evaluated benchmarks. The gains range from approximately 3.5–8% in the 2 Å & PB-validity metric. Notably, these improvements are achieved with a substantially smaller model:  $\sim 638k$  parameters for MolAS versus  $\sim 3.2M$  for MC-GNNAS-Dock. This suggests that in the current data regime,

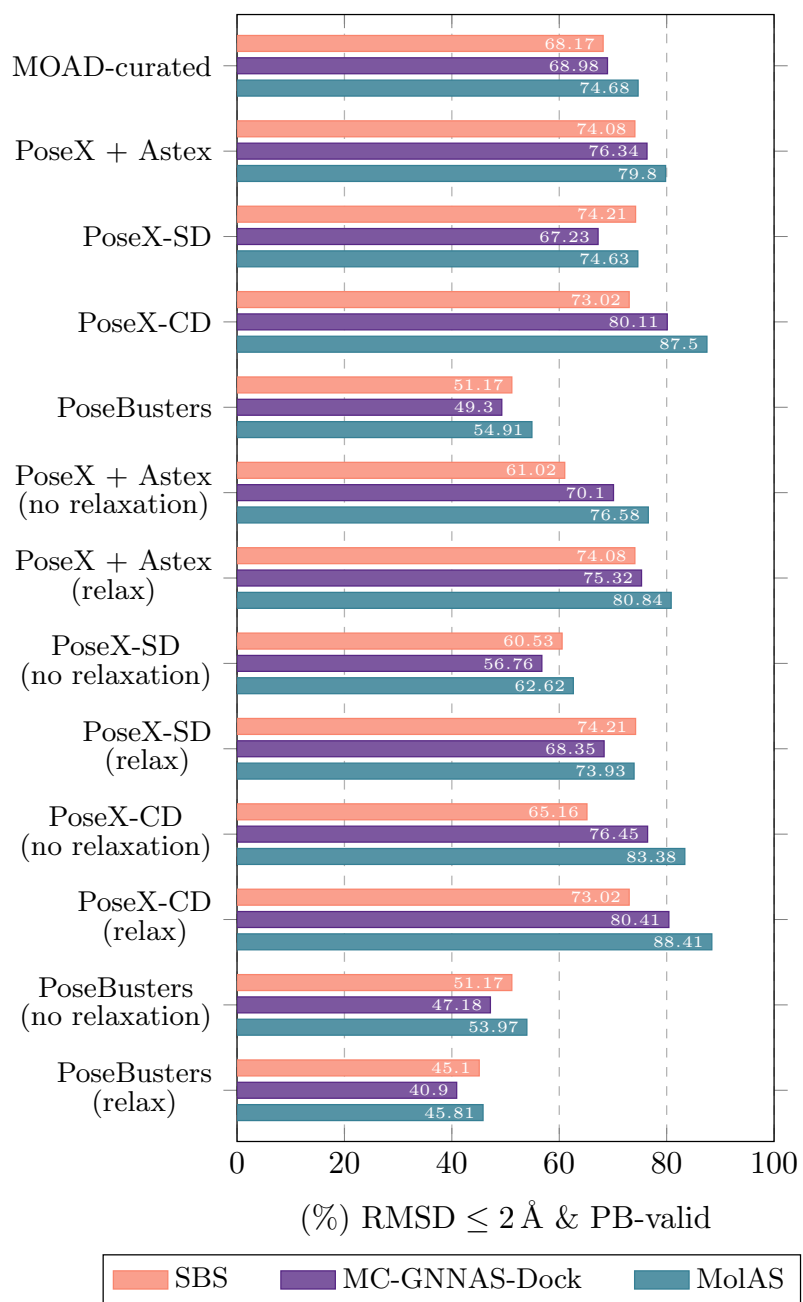


**Fig. 9** Comparison among SBS, MC-GNNAS-Dock, and MolAS in averaged 5-fold results in in PoseBusters-validated pose rate within 2 Å RMSD across benchmarks.

**Table 4** Component-wise ablation of architectural modules and optimisation objectives based on the MolAS baseline, with the default choices indicated in the brackets.  $\uparrow$  denotes improvements over MolAS and  $\downarrow$  denotes declinations.

Ablated items	% $\leq x$ Å & PB-valid			
	MOAD-curated		PoseX + Astex	
	$x = 1$	$x = 2$	$x = 1$	$x = 2$
<b>SBS</b>	43.41	68.17	50.24	74.08
<b>MolAS</b>	50.01	74.68	58.61	79.80
<b>GNN encoder (MolAS: None)</b>				
GCN-GAT-GINE	48.38 $\downarrow$	71.34 $\downarrow$	56.81 $\downarrow$	78.81 $\downarrow$
EGNN-GAT-GINE	47.37 $\downarrow$	71.81 $\downarrow$	57.19 $\downarrow$	78.67 $\downarrow$
<b>Protein attention heads (MolAS: 1)</b>				
2	48.22 $\downarrow$	72.70 $\downarrow$	58.37 $\downarrow$	79.90 $\uparrow$
4	49.01 $\downarrow$	72.92 $\downarrow$	58.70 $\uparrow$	79.85 $\uparrow$
<b>Decoder (MolAS: 4 ResBlock(128, 256))</b>				
6 ResBlock(128, 256)	48.19 $\downarrow$	71.75 $\downarrow$	59.93 $\uparrow$	80.27 $\uparrow$
2 ResBlock(128, 256)	47.81 $\downarrow$	71.56 $\downarrow$	59.13 $\uparrow$	80.37 $\uparrow$
4 ResBlock(256, 512)	48.79 $\downarrow$	72.29 $\downarrow$	58.23 $\downarrow$	79.28 $\downarrow$
4 ResBlock(64, 128)	48.57 $\downarrow$	71.94 $\downarrow$	57.71 $\downarrow$	80.42 $\uparrow$
Single linear layer	48.88 $\downarrow$	72.57 $\downarrow$	59.84 $\uparrow$	80.98 $\uparrow$
<b>Scoring function (MolAS: <math>\lambda = 3</math>)</b>				
$\lambda = 1$	48.75 $\downarrow$	70.75 $\downarrow$	60.12 $\uparrow$	78.01 $\downarrow$
$\lambda = 5$	48.48 $\downarrow$	72.85 $\downarrow$	57.52 $\downarrow$	80.80 $\uparrow$
<b>Ranking-aware loss (MolAS: BCE)</b>				
BCE + PL	48.50 $\downarrow$	71.47 $\downarrow$	59.65 $\uparrow$	77.15 $\downarrow$
BCE + NDCG@3	48.47 $\downarrow$	72.32 $\downarrow$	59.70 $\uparrow$	80.51 $\uparrow$
BCE + PL + NDCG@3	48.22 $\downarrow$	71.25 $\downarrow$	60.12 $\uparrow$	78.01 $\downarrow$

lightweight embedding-level architectures exploit available signal more efficiently than deeper graph-based models, aligning with the earlier ablation results that point to a data-limited rather than architecture-limited setting.

### 3.3 Ablation

Ablations, detailed in Table 4, across the two major benchmark sets, *MOAD-curated* and *PoseX + Astex*, were conducted to examine the optimality and robustness of MolAS. Parallel GNN encoder stacks (GCN-GAT-GINE, inspired by graphLambda [Mqawass and Popov, 2024], and an equivariant EGNN-GAT-GINE variant) failed to surpass over the embedding-only model, indicating that residue-level ESM-C representations already capture the structural signal required in this data regime. Increasing the number of attention heads produced only sub-percentage fluctuations with no consistent pattern. Decoder capacity exhibited a similarly limited effect, with deeper or wider residual stacks yielding only marginal gains on one benchmark at the expense of performance on the other. A single linear decoder achieved peak

performance on the *PoseX + Astex* set under the 2 Å & PB-validity criterion. However, its performance on the *MOAD-curated* benchmark decreased by approximately 2%. This suggests the current residual decoder introduces partial redundancy and that exploiting larger architectures will require additional data rather than increased depth.

Sensitivity to the scoring-function hyperparameter was modest: altering the RMSD–validity trade-off from  $\lambda = 3$  to  $\lambda = 1$  or 5 shifted scores by at most 2%, and the directions of change differed across benchmarks, implying that MolAS is relatively insensitive to reasonable weighting choices. Ranking-aware objectives, including pairwise logistic (PL), Normalized Discounted Cumulative Gain (NDCG@)3, and their combination with BCE, likewise produced only noise-level variation, with no systematic gain. The overall performance spread across all ablations remained within  $\sim 2\%$ , underscoring that none of the architectural or objective-function modifications meaningfully changed the behaviour of the model.

Taken together, these results support a clear interpretation that MolAS is *data-limited* rather than *architecture-limited*. Additional architectural complexity fails to yield reliable improvements. The baseline configuration therefore represents an appropriate balance of expressiveness and stability for the scale and heterogeneity of the available data.

## 4 Discussion

### 4.1 Stability, failures, and workflow dependence

MolAS is not a universal docking selector but a benchmark-dependent model whose performance closely tracks the stability of the underlying oracle hierarchy. In regimes with genuinely diverse solver competency, such as *MOAD-curated* and *PoseX-CD*, MolAS consistently closes 17-66% of the VBS–SBS gap and saturates within hundred to a few thousand labelled complexes. This indicates that residue-level ESM C and ligand ChemBERTa embeddings already encode most of the discriminative signal needed for in-domain selection.

Failures occur when solvers are poorly separated in embedding space or when the SBS dominates the oracle landscape. In such cases, MolAS converges to a near-constant, SBS-like policy that is locally reasonable but globally suboptimal. Cross-benchmark transfers show a similar pattern: changes in pose-generation alter the oracle hierarchy and effectively redefine the AS task, leading to systematic negative transfer and even widening of the VBS–SBS gap. These observations are consistent with our oracle-geometry diagnostics: benchmark differences primarily manifest as changes in oracle entropy and embedding separability rather than as simple shifts in marginal difficulty.

From a practical perspective, MolAS remains attractive when the workflow is fixed. Once the algorithm portfolio, data distribution, and post-processing regime are specified, the selector reaches stable gap-closing performance with modest labelling effort and can be deployed as a lightweight plug-in on top of existing docking pipelines.

## 4.2 Implications and limitations for docking AS

The experiments collectively rule out representation capacity as the main bottleneck for docking AS at current data scales. Architectural scaling, from small MLPs through GNN stacks, failed to deliver systematic gains beyond what pretrained embeddings and a shallow decoder already achieve. Instead, the limiting factors are the diversity and separability of multi-algorithm labels and protocol-induced shifts in solver rankings. Any selector that is trained purely on molecular inputs but evaluated under changing docking workflows is, by construction, trying to approximate an oracle that is not invariant.

## 4.3 Future directions

Future advancements will require coordinated development across several areas. Incorporating explicit protocol data may help stabilise the selector under minor regime changes. More principled confidence/uncertainty estimation could reduce winner-take-all failures when the embedding geometry offers weak separation between solvers. Ultimately, cross-protocol generalisation is unlikely to be achievable without standardising evaluation pipelines or explicitly modelling shifts in oracle structure. These considerations define a realistic scope for algorithm selection in docking and identify where methodological work is most likely to have impact.

### Abbreviations

AS	Algorithm selection
BCE	Binary cross-entropy
CD	Cross docking
EGNN	Equivariant graph neural network
GAT	Graph attention network
GINE	Graph isomorphism network
GNN	Graph neural network
ML	Machine learning
MM-min	Molecular-mechanics energy minimisation
MolAS	Molecular embedding-based algorithm selector
NDCG	Normalized Discounted Cumulative Gain
PB	PoseBusters
PL	Pairwise logistic
RMSD	Root-mean-square deviation
SBS	Single best solver
SD	Self docking
VBS	Virtual best solver

### Declarations

**Availability of data and materials.** The dataset supporting the conclusions of this article including processed complexes, per-algorithm performances, and in-domain checkpoints is available on Zenodo at <https://zenodo.org/records/17760688>. The codes

for generating embeddings, training and testing MolAS are available in the MolAS GitHub repository at <https://github.com/BradWangW/MolAS>.

**Competing interests.** No competing interest is declared.

**Funding.** Not applicable.

**Authors’ contributions.** Y.Y. developed the base GNNAS-Dock framework. S.C. and H.W. designed and implemented the MC-GNNAS-Dock extensions with input from all authors. J.B.W. performed the MolAS experiments and analyses and drafted the manuscript. M.M. conceptualised the research direction, supervised all experiments and analyses, and edited the manuscript. All authors reviewed and approved the final version.

**Acknowledgements.** The research results of this article are sponsored by the Wang-Cai Biochemistry Lab and Syneer Food Molecular Biology Lab.

Editorial Policies for:

Springer journals and proceedings: <https://www.springer.com/gp/editorial-policies>

Nature Portfolio journals: <https://www.nature.com/nature-research/editorial-policies>

*Scientific Reports*: <https://www.nature.com/srep/journal-policies/editorial-policies>

BMC journals: <https://www.biomedcentral.com/getpublished/editorial-policies>

## Appendix A Appendix

### A.1 Verbose results

Detailed performances over algorithm portfolios and MolAS/VBS selection frequencies over *MOAD-curated*, *PoseX + Astex*, *PoseX-SD*, *PoseX-CD*, and *PoseBusters* are shown in Figures [A1](#), [A2](#), [A3](#), [A4](#), and [A5](#).

## References

- Walid Ahmad, Elana Simon, Seyone Chithrananda, Gabriel Grand, and Bharath Ramsundar. Chemberta-2: Towards chemical foundation models. *arXiv preprint arXiv:2209.01712*, 2022.
- Eric Alcaide, Zhifeng Gao, Guolin Ke, Yaqi Li, Linfeng Zhang, Hang Zheng, and Gengmo Zhou. Uni-mol docking v2: Towards realistic and accurate binding pose prediction. In *International Conference on Artificial Neural Networks*, pages 34–41. Springer, 2025. doi: 10.1007/978-3-032-04552-2\_5.
- Pedro J Ballester and John BO Mitchell. A machine learning approach to predicting protein–ligand binding affinity with applications to molecular docking. *Bioinformatics*, 26(9):1169–1175, 2010. doi: 10.1093/bioinformatics/btq112.

(a) Averaged 5-fold results on MOAD-curated.

Method	(%) RMSD $\leq x$ Å & PB-valid	
	$x = 1$	$x = 2$
<b>Physics-based methods</b>		
Qvina-W	11.20	19.28
Smina	11.23	19.50
GNINA	25.45	42.87
(hybrid)		
<b>AI docking methods</b>		
KarmaDock	3.08	8.50
DiffDock	8.60	11.40
DiffDock-L	10.22	14.72
SurfDock	39.28	53.66
Uni-Mol	<b>43.41</b>	<b>68.16</b>
<b>MolAS</b>	<b>50.01</b>	<b>74.68</b>
VBS@1	81.31	97.23
VBS@2	69.20	95.56
VBS@3	50.96	84.11

(b) (%) Selection frequencies on MOAD-curated.

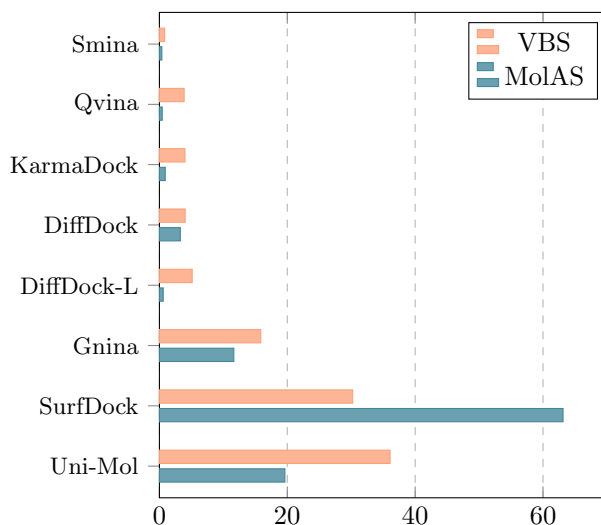


**Fig. A1** Table of performances over the algorithm portfolio (left) and histogram of MolAS/VBS selection frequencies (right) on **MOAD-curated**. In the table, the portfolio-wise best and MolAS performances are in **bold**. Performances are ordered by ascending percentage of poses below 2 Å and PoseBusters-valid, while frequencies are ordered by ascending VBS frequency.

- Martin Buttenschoen, Garrett M Morris, and Charlotte M Deane. Posebusters: Ai-based docking methods fail to generate physically valid poses or generalise to novel sequences. *Chemical Science*, 15(9):3130–3139, 2024. doi: 10.1039/D3SC04185A.
- Duanhua Cao, Mingan Chen, Runze Zhang, Zhaokun Wang, Manlin Huang, Jie Yu, Xinyu Jiang, Zhehuan Fan, Wei Zhang, Hao Zhou, et al. Surfdock is a surface-informed diffusion generative model for reliable and accurate protein–ligand complex prediction. *Nature Methods*, 22(2):310–322, 2025a. doi: 10.1038/s41592-024-02516-y.
- Siyuan Cao, Hongxuan Wu, Jiabao Brad Wang, Yiliang Yuan, and Mustafa Misir. Mc-gnnas-dock: Multi-criteria gnn-based algorithm selection for molecular docking. *arXiv preprint arXiv:2509.26377*, 2025b.
- Tianlai Chen, Xiwen Shu, Huiyuan Zhou, Floyd A Beckford, and Mustafa Misir. Algorithm selection for protein–ligand docking: strategies and analysis on ace. *Scientific Reports*, 13(1):8219, 2023. doi: 10.1038/s41598-023-35132-5.
- Tiejun Cheng, Zhihai Liu, and Renxiao Wang. A knowledge-guided strategy for improving the accuracy of scoring functions in binding affinity prediction. *BMC bioinformatics*, 11(1):193, 2010. doi: 10.1186/1471-2105-11-193.
- Gabriele Corso, Hannes Stärk, Bowen Jing, Regina Barzilay, and Tommi Jaakkola. Diffdock: Diffusion steps, twists, and turns for molecular docking. *arXiv preprint arXiv:2210.01776*, 2022.
- Gabriele Corso, Arthur Deng, Benjamin Fry, Nicholas Polizzi, Regina Barzilay, and Tommi Jaakkola. Deep confident steps to new pockets: Strategies for docking generalization. *arXiv preprint arXiv:2402.18396*, 2024.



Averaged 5-fold results on PoseX + Astex.

Method	(%) RMSD $\leq x$ Å & PB-valid	
	$x = 1$	$x = 2$
<b>Physics-based methods</b>		
AutoDock Vina	17.170	31.502
AutoDock Vina (relax)	18.496	33.112
MOE (relax)	18.258	33.350
MOE	18.258	33.822
Schrödinger Glide (relax)	22.186	39.262
Schrödinger Glide	21.098	39.498
Glide (IFD)	20.718	41.910
Glide (IFD) (relax)	21.284	41.912
Discovery Studio (relax)	27.722	45.788
Discovery Studio	27.672	46.356
GNINA (hybrid)	25.544	53.310
GNINA (hybrid) (relax)	27.340	56.054
<b>AI docking methods</b>		
EquiBind	0.000	0.618
FABind	1.938	4.778
TankBind	2.268	5.346
DeepDock	2.364	6.054
EquiBind (relax)	1.088	6.480
DynamicBind	5.060	9.510
DeepDock (relax)	5.346	15.656
TankBind (relax)	7.380	18.402
DiffDock	13.860	23.180
FABind (relax)	9.462	23.274
DiffDock-L	21.054	30.038
DynamicBind (relax)	14.002	33.062
DiffDock-Pocket	21.806	35.144
SurfDock	32.024	39.782
Interformer	22.326	42.382
DiffDock (relax)	25.214	44.796
DiffDock-L (relax)	33.348	50.946
DiffDock-Pocket (relax)	32.214	56.384
Uni-Mol	37.654	57.900
Uni-Mol (relax)	37.656	57.948
Interformer (relax)	31.500	58.606
SurfDock (relax)	<b>50.236</b>	<b>74.078</b>
<b>AI co-folding methods</b>		
NeuralPLexer	0.522	1.986
RFAA	4.350	7.806
NeuralPLexer (relax)	5.772	18.068
RFAA (relax)	10.358	24.218
Boltz-1	30.842	43.710
Protenix	35.006	48.532
Protenix (relax)	36.566	51.422
Chai-1	39.450	51.988
Boltz-1 (relax)	36.142	53.124
AlphaFold 3	42.904	54.778
Chai-1 (relax)	42.384	57.428
AlphaFold 3 (relax)	44.416	59.462
Boltz-1x	42.478	61.022
Boltz-1x (relax)	41.104	61.070
<b>MolAS</b>	<b>58.606</b>	<b>79.800</b>
VBS@1	89.308	97.684
VBS@2	86.896	97.256
VBS@3	82.022	95.222

(%) Selection frequencies on PoseX + Astex.

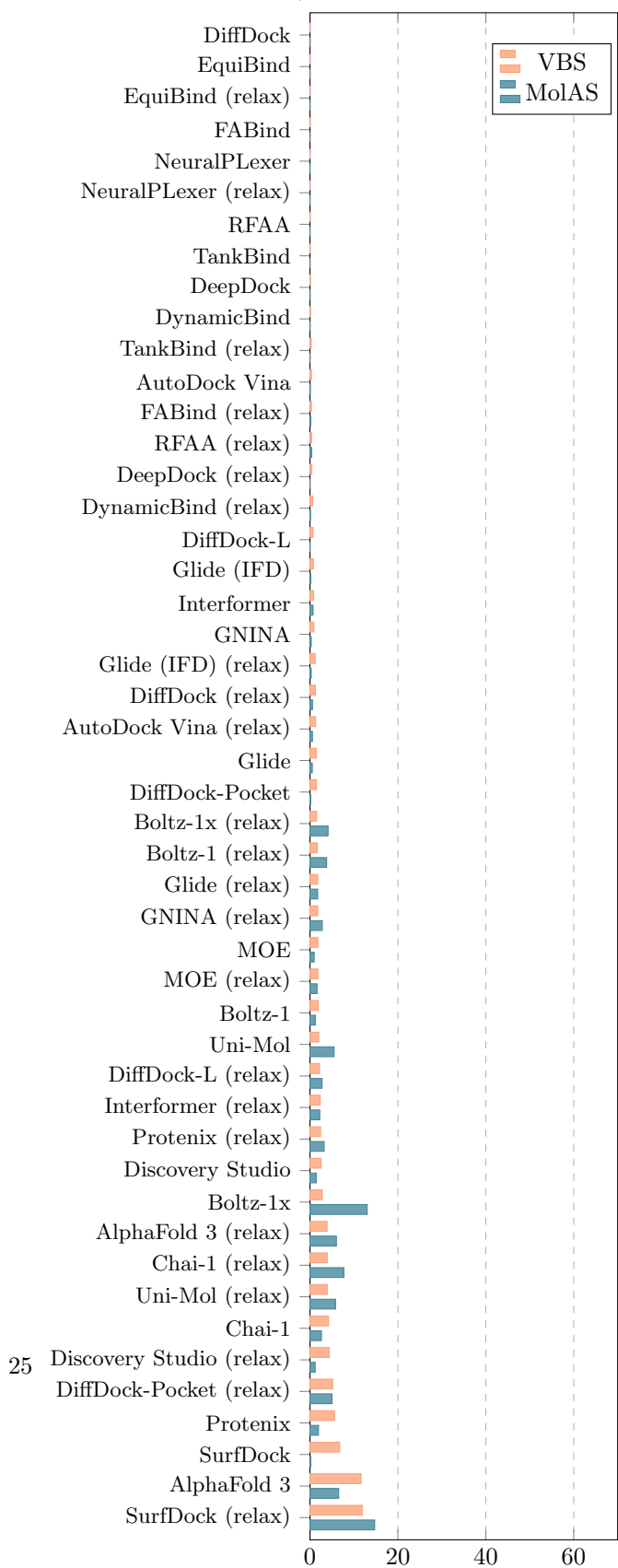


**Fig. A2** Table of performances over the algorithm portfolio (left) and histogram of MolAS/VBS selection frequencies (right) on PoseX + Astex. In the table, the portfolio-wise best and MolAS performances are in **bold**. Performances are ordered by ascending percentage of poses below 2 Å and PoseBusters-valid, while frequencies are ordered by ascending VBS frequency.

Averaged 5-fold results on PoseX-SD.

Method	(%) RMSD $\leq x$ Å & PB-valid	
	$x = 1$	$x = 2$
<b>Physics-based methods</b>		
AutoDock Vina	22.590	36.812
MOE (relax)	23.160	37.670
AutoDock Vina (relax)	23.708	38.348
MOE	23.716	39.474
Glide (IFD) (relax)	24.822	45.460
Glide (IFD)	26.216	46.156
Schrödinger Glide (relax)	31.380	46.292
Schrödinger Glide	30.826	47.966
Discovery Studio (relax)	35.714	52.584
Discovery Studio	36.554	53.976
GNINA (hybrid)	33.472	59.558
GNINA (hybrid) (relax)	34.030	61.788
<b>AI docking methods</b>		
EquiBind	0.000	0.420
FABind	1.254	2.092
TankBind	1.394	4.186
EquiBind (relax)	0.558	4.326
DeepDock	3.348	6.410
DynamicBind	3.624	7.810
FABind (relax)	4.464	12.690
TankBind (relax)	5.022	12.834
DeepDock (relax)	5.720	15.058
DiffDock	9.342	16.034
DiffDock-L	17.428	25.102
DynamicBind (relax)	11.012	25.518
DiffDock-Pocket	18.684	29.006
DiffDock (relax)	17.986	34.588
SurfDock	32.506	41.578
DiffDock-L (relax)	29.426	44.770
Interformer	24.402	48.108
DiffDock-Pocket (relax)	27.334	49.510
Uni-Mol (relax)	39.474	59.140
Uni-Mol	40.730	60.530
Interformer (relax)	34.312	63.316
SurfDock (relax)	<b>50.078</b>	<b>74.210</b>
<b>AI co-folding methods</b>		
NeuralPLexer	0.698	1.396
RFAA	4.180	7.106
NeuralPLexer (relax)	5.572	15.612
RFAA (relax)	12.126	27.052
Boltz-1	25.660	34.306
Boltz-1 (relax)	29.142	42.392
Chai-1	33.054	43.654
Protenix	34.592	44.770
AlphaFold 3	34.730	45.468
Protenix (relax)	35.706	47.700
Chai-1 (relax)	35.566	49.512
Boltz-1x (relax)	34.866	51.880
AlphaFold 3 (relax)	38.354	51.886
Boltz-1x	36.114	52.300
<b>MolAS</b>	<b>51.616</b>	<b>74.628</b>
VBS@1	92.052	99.304
VBS@2	89.540	99.304
VBS@3	85.216	97.072

(%) Selection frequencies on PoseX-SD.

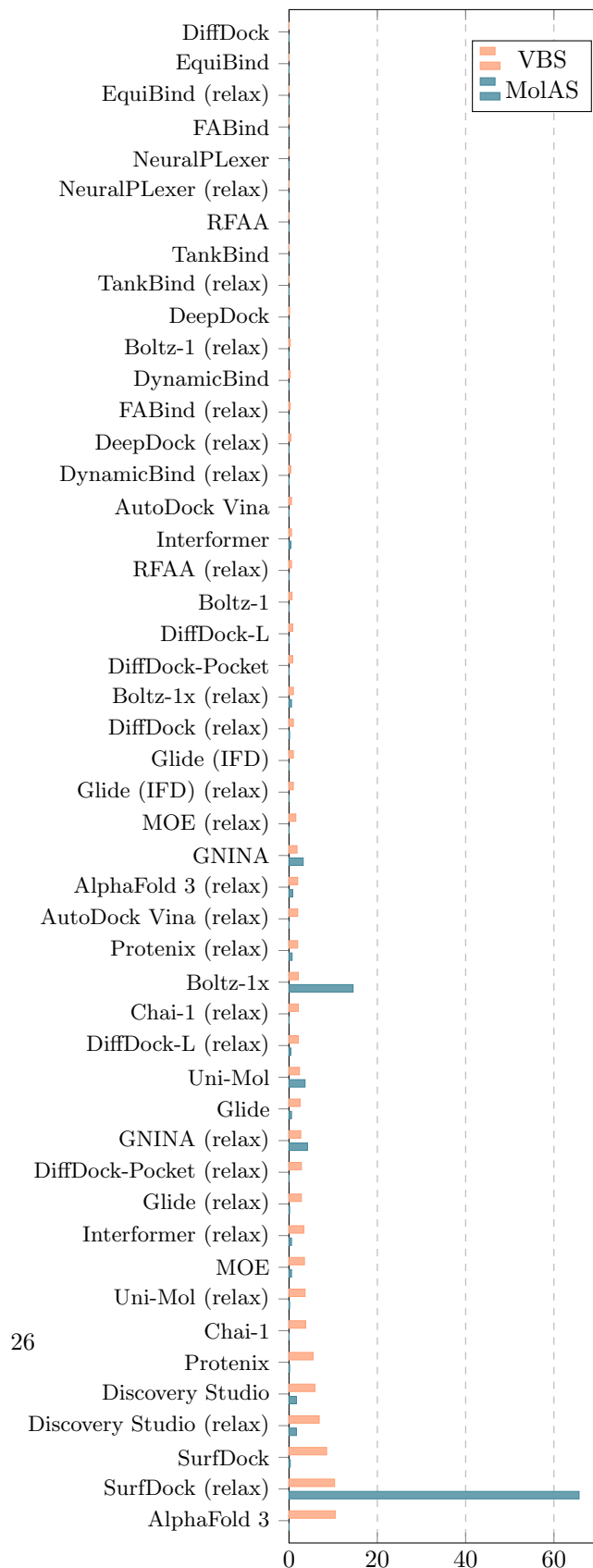


**Fig. A3** Table of performances over the algorithm portfolio (left) and histogram of MolAS/VBS selection frequencies (right) on **PoseX-SD**. In the table, the portfolio-wise best and MolAS performances are in **bold**. Performances are ordered by ascending percentage of poses below 2 Å and PoseBusters-valid, while frequencies are ordered by ascending VBS frequency.

Averaged 5-fold results on PoseX-CD.

Method	(%) RMSD $\leq x$ Å & PB-valid	
	$x = 1$	$x = 2$
<b>Physics-based methods</b>		
AutoDock Vina	13.338	27.288
AutoDock Vina (relax)	14.634	28.810
MOE	13.870	29.270
MOE (relax)	14.178	29.422
Glide	14.710	33.306
Glide (relax)	16.006	33.840
Glide (IFD)	17.230	37.958
Glide (IFD) (relax)	18.602	38.338
Discovery Studio (relax)	22.252	40.850
Discovery Studio	21.642	40.924
GNINA (hybrid)	19.740	48.088
GNINA (hybrid) (relax)	22.408	51.290
<b>AI docking methods</b>		
EquiBind	0.000	0.608
DeepDock	1.600	5.560
FABind	1.906	5.942
TankBind	2.744	5.944
EquiBind (relax)	1.450	7.470
DynamicBind	5.486	9.758
DeepDock (relax)	4.802	15.474
TankBind (relax)	8.078	20.502
DiffDock	13.948	24.620
FABind (relax)	11.506	28.582
DiffDock-L	19.964	29.950
DynamicBind (relax)	14.788	35.522
DiffDock-Pocket	21.494	36.888
SurfDock	30.414	37.350
Interformer	19.664	38.106
DiffDock (relax)	26.904	48.470
DiffDock-L (relax)	32.540	52.128
Interformer (relax)	28.046	54.572
Uni-Mol	33.382	54.648
Uni-Mol (relax)	33.916	55.562
DiffDock-Pocket (relax)	32.238	58.382
SurfDock (relax)	<b>49.080</b>	<b>73.016</b>
<b>AI co-folding methods</b>		
NeuralPLexer	0.456	2.436
RFAA	4.264	8.080
NeuralPLexer (relax)	5.412	18.598
RFAA (relax)	9.298	22.102
Boltz-1	32.700	48.244
Protenix	33.456	49.384
Protenix (relax)	35.208	52.130
Chai-1	41.312	55.338
AlphaFold 3	45.808	58.534
Boltz-1 (relax)	39.248	58.686
Chai-1 (relax)	44.742	60.670
AlphaFold 3 (relax)	46.264	62.500
Boltz-1x	44.816	65.162
Boltz-1x (relax)	43.520	65.390
<b>MolAS</b>	<b>66.386</b>	<b>87.496</b>
VBS@1	87.114	96.646
VBS@2	84.598	95.960
VBS@3	79.264	93.900

(%) Selection frequencies on PoseX-CD.

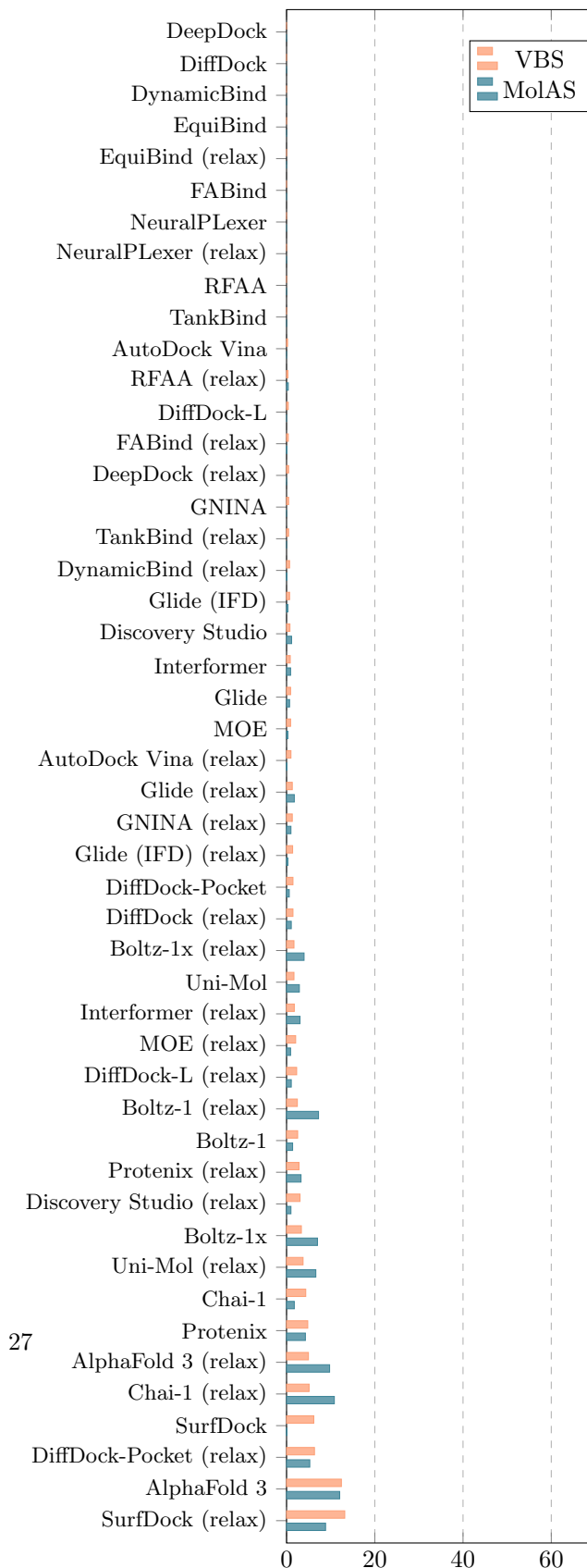


**Fig. A4** Table of performances over the algorithm portfolio (left) and histogram of MolAS/VBS selection frequencies (right) on **PoseX-CD**. In the table, the portfolio-wise best and MolAS performances are in **bold**. Performances are ordered by ascending percentage of poses below 2 Å and PoseBusters-valid, while frequencies are ordered by ascending VBS frequency.

(c) Averaged 5-fold results on PoseBusters.

Method	(%) RMSD $\leq x$ Å & PB-valid	
	$x = 1$	$x = 2$
<b>Physics-based methods</b>		
AutoDock Vina (MM-min)	28.724	44.150
GOLD (MM-min)	27.582	45.102
GOLD	32.712	48.364
AutoDock Vina	<b>34.338</b>	<b>51.166</b>
<b>AI docking methods</b>		
EquiBind	0.000	0.704
Uni-Mol	1.400	2.096
TankBind	0.936	2.570
DeepDock	2.572	4.910
EquiBind (MM-min)	2.342	7.488
DiffDock	8.888	14.026
TankBind (MM-min)	5.842	14.252
DeepDock (MM-min)	6.544	15.188
Uni-Mol (MM-min)	7.944	19.848
DiffDock (MM-min)	17.052	35.982
<b>MolAS</b>	<b>36.688</b>	<b>54.910</b>
VBS@1	60.750	82.714
VBS@2	48.600	78.746
VBS@3	38.312	68.004

(d) (%) Selection frequencies on PoseBusters.

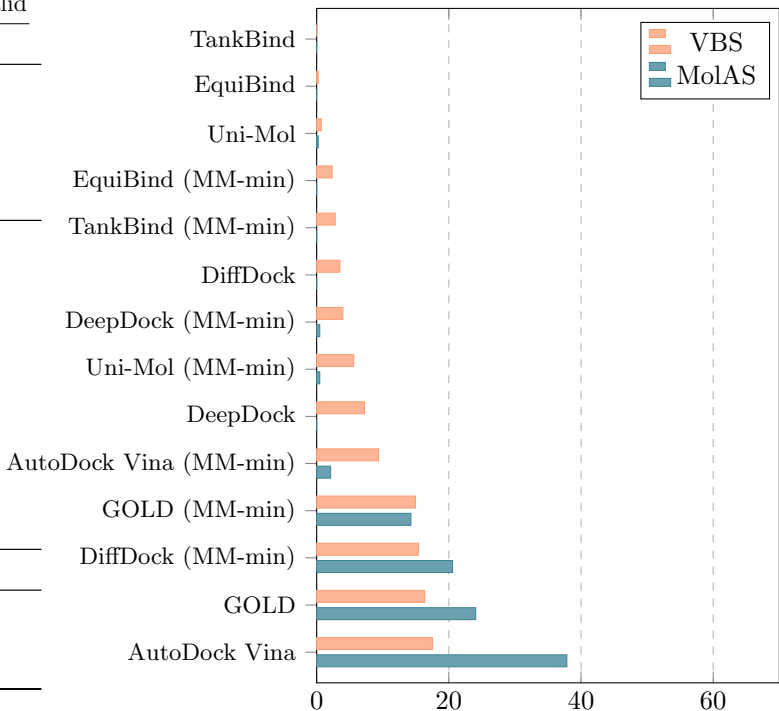


**Fig. A5** Table of performances over the algorithm portfolio (left) and histogram of MolAS/VBS selection frequencies (right) on **PoseBusters**. In the table, the portfolio-wise best and MolAS performances are in **bold**. Performances are ordered by ascending percentage of poses below 2 Å and PoseBusters-valid, while frequencies are ordered by ascending VBS frequency.

ESM Team. Esm cambrian: Revealing the mysteries of proteins with unsupervised learning, 2024. URL <https://evolutionaryscale.ai/blog/esm-cambrian>.

Jiyu Fan, Ailing Fu, and Le Zhang. Progress in molecular docking. *Quantitative Biology*, 7(2):83–89, 2019. doi: 10.1007/s40484-019-0172-y.

Matthias Feurer, Aaron Klein, Katharina Eggensperger, Jost Springenberg, Manuel Blum, and Frank Hutter. Efficient and robust automated machine learning. *Advances in neural information processing systems*, 28, 2015. URL [https://proceedings.neurips.cc/paper\\_files/paper/2015/file/11d0e6287202fcd83f79975ec59a3a6-Paper.pdf](https://proceedings.neurips.cc/paper_files/paper/2015/file/11d0e6287202fcd83f79975ec59a3a6-Paper.pdf).

Paul G Francoeur, Tomohide Masuda, Jocelyn Sunseri, Andrew Jia, Richard B Iovanisci, Ian Snyder, and David R Koes. Three-dimensional convolutional neural networks and a cross-docked data set for structure-based drug design. *Journal of chemical information and modeling*, 60(9):4200–4215, 2020. doi: 10.1021/acs.jcim.0c00411.

- Michael J Hartshorn, Marcel L Verdonk, Gianni Chessari, Suzanne C Brewerton, Wijnand TM Mooij, Paul N Mortenson, and Christopher W Murray. Diverse, high-quality test set for the validation of protein-ligand docking performance. *Journal of medicinal chemistry*, 50(4):726–741, 2007. doi: 10.1021/jm061277y.
- Nafisa M Hassan, Amr A Alhossary, Yuguang Mu, and Chee-Keong Kwoh. Protein-ligand blind docking using quickvina-w with inter-process spatio-temporal integration. *Scientific reports*, 7(1):15451, 2017. doi: 10.1038/s41598-017-15571-7.
- Fengxiang He, Tongliang Liu, and Dacheng Tao. Why resnet works? residuals generalize. *IEEE transactions on neural networks and learning systems*, 31(12):5349–5362, 2020. doi: 10.1109/TNNLS.2020.2966319.
- Liegi Hu, Mark L Benson, Richard D Smith, Michael G Lerner, and Heather A Carlson. Binding moad (mother of all databases). *Proteins: Structure, Function, and Bioinformatics*, 60(3):333–340, 2005. doi: 10.1002/prot.20512.
- Yize Jiang, Xinze Li, Yuanyuan Zhang, Jin Han, Youjun Xu, Ayush Pandit, ZAI XI ZHANG, Mengdi Wang, Mengyang Wang, Chong Liu, Guang Yang, Yejin Choi, Wu-Jun Li, Tianfan Fu, Fang Wu, and Junhong Liu. Posex: AI defeats physics-based methods on protein ligand cross-docking, 2025. URL <https://openreview.net/forum?id=qHOU1aAyXA>.
- Pascal Kerschke, Holger H Hoos, Frank Neumann, and Heike Trautmann. Automated algorithm selection: Survey and perspectives. *Evolutionary computation*, 27(1):3–45, 2019. doi: 10.1162/evco.a\_00242.
- David Ryan Koes, Matthew P Baumgartner, and Carlos J Camacho. Lessons learned in empirical scoring with smina from the csar 2011 benchmarking exercise. *Journal of chemical information and modeling*, 53(8):1893–1904, 2013. doi: 10.1021/ci300604z.
- Zeming Lin, Chetan Mishra, santiag0m, Jun Gong, Neil Thomas, Ishaan Mathur, tina-z jia, Tom Sercu, Steve Chan, Salvatore Candido, Jenna MacCarley, Imran Qureshi, Jordan Safer, robert verkuil, Ventura Rivera, blenderwang, carolynkim, and halilakin. evolutionaryscale/esm: v3.2.3, October 2025. URL <https://doi.org/10.5281/zenodo.17353381>.
- Zhihai Liu, Minyi Su, Li Han, Jie Liu, Qifan Yang, Yan Li, and Renxiao Wang. Forging the basis for developing protein-ligand interaction scoring functions. *Accounts of chemical research*, 50(2):302–309, 2017. doi: 10.1021/acs.accounts.6b00491.
- Andrew T McNutt, Paul Francoeur, Rishal Aggarwal, Tomohide Masuda, Rocco Meli, Matthew Ragoza, Jocelyn Sunseri, and David Ryan Koes. Gnina 1.0: molecular docking with deep learning. *Journal of cheminformatics*, 13(1):43, 2021. doi: 10.1186/s13321-021-00522-2.
- Xuan-Yu Meng, Hong-Xing Zhang, Mihaly Mezei, and Meng Cui. Molecular docking: a powerful approach for structure-based drug discovery. *Current computer-aided drug design*, 7(2):146–157, 2011. doi: 10.2174/157340911795677602.
- Mustafa Misir and Michèle Sebag. Alors: An algorithm recommender system. *Artificial Intelligence*, 244:291–314, 2017. doi: 10.1016/j.artint.2016.12.001.
- Ghaith Mqawass and Petr Popov. graphlambda: fusion graph neural networks for binding affinity prediction. *Journal of Chemical Information and Modeling*, 64(7):2323–2330, 2024. doi: 10.1021/acs.jcim.3c00771.

- Ivan Olier, Nouredin Sadawi, G Richard Bickerton, Joaquin Vanschoren, Crina Grosan, Larisa Soldatova, and Ross D King. Meta-qsar: a large-scale application of meta-learning to drug design and discovery. *Machine Learning*, 107(1):285–311, 2018. doi: 10.1007/s10994-017-5685-x.
- John R Rice. The algorithm selection problem. In *Advances in computers*, volume 15, pages 65–118. Elsevier, 1976. doi: 10.1016/S0065-2458(08)60520-3.
- Minyi Su, Qifan Yang, Yu Du, Guoqin Feng, Zhihai Liu, Yan Li, and Renxiao Wang. Comparative assessment of scoring functions: the casf-2016 update. *Journal of chemical information and modeling*, 59(2):895–913, 2018. doi: 10.1021/acs.jcim.8b00545.
- Chris Thornton, Frank Hutter, Holger H Hoos, and Kevin Leyton-Brown. Auto-weka: Combined selection and hyperparameter optimization of classification algorithms. In *Proceedings of the 19th ACM SIGKDD international conference on Knowledge discovery and data mining*, pages 847–855, 2013. doi: 10.1145/2487575.2487629.
- Oleg Trott and Arthur J Olson. Autodock vina: improving the speed and accuracy of docking with a new scoring function, efficient optimization, and multithreading. *Journal of computational chemistry*, 31(2):455–461, 2010. doi: 10.1002/jcc.21334.
- David H Wolpert and William G Macready. No free lunch theorems for optimization. *IEEE transactions on evolutionary computation*, 1(1):67–82, 2002. doi: 10.1109/4235.585893.
- Yiliang Yuan and Mustafa Misir. Algorithm selection on molecular docking for state-of-the-art performance. In *Proceedings of the 2024 8th International Conference on Computer Science and Artificial Intelligence*, pages 295–302, 2024a. doi: 10.1145/3709026.3709046.
- Yiliang Yuan and Mustafa Misir. Enhancing molecular docking performance with a gnn-based algorithm selection model. In *Proceedings of the 2024 8th International Conference on Computational Biology and Bioinformatics*, pages 14–19, 2024b. doi: 10.1145/3715020.3715040.
- Yiliang Yuan and Mustafa Misir. Gnnas-dock: Budget aware algorithm selection with graph neural networks for molecular docking. In *NeurIPS 2024 Workshop on AI for New Drug Modalities*, 2024c. URL <https://openreview.net/forum?id=W4d1a4odSc>.
- Ala’Omar Hasan Zayed. Optimizing protein-ligand docking through machine learning: algorithm selection with autodock vina. *Discover Chemistry*, 2(1):164, 2025. doi: 10.1007/s44371-025-00246-4.
- Xujun Zhang, Odin Zhang, Chao Shen, Wanglin Qu, Shicheng Chen, Hanqun Cao, Yu Kang, Zhe Wang, Ercheng Wang, Jintu Zhang, et al. Efficient and accurate large library ligand docking with karmadock. *Nature Computational Science*, 3(9):789–804, 2023. doi: 10.1038/s43588-023-00511-5.